Modeling and design of magnetic shields for electrical Installations

POLITECNICO DI TORINO

Phd in Electrical engineering

TITLE

Modeling and design of magnetic shields for electrical Installations

Rapporteurs:

Prof. Aldo Canova

Ing. Luca Giaccone

Candidate: Ing. Davide Bavastro

Turin, January 2014

1 Introduction 3
2 Formulation 6
2.1 Sources 6
2.1.1 Straight conductor segment in space: 6
2.1.2 Toroidal winding in the space 9
2.2 Application of symbolic method for sinusoidal currents 13
2.2.1 Implementation of the model of the transformer 14
2.3 Shielding system 20
2.3.1 Ferromagnetic Materials 21
2.3.2 Conductive Materials 23
2.3.3 Multilayer shield 38
3 Set Up of the laboratory tests 40
3.1 Generator for the testing of power lines and MV, LV switchgears 40
3.1.1 Architecture 40
3.1.2 Realization 45
3.2 Generator for the testing of MV/LV Transformer 49
4 Results and Comparisons 52
4.1 Shielding of a box office of a car wash 53
4.1.1 Computation of the values of magnetic induction produced by the line 54
4.1.2 Design of the shielding system 55
4.1.3 Result of the simulations 56
4.1.4 Implementation of the shielding system 59
4.1.5 Check of the shielding factor 60
4.1.6 Validation of the computation code and conclusion 61
4.2 Shielding of the doors of a particular electrical cabinet 63
4.2.1 Design of the shielding system 65
4.2.2 Result of the simulations 68
4.2.3 Conclusion 73
4.3 Shielding of a public office under a substation MV/LV 74
4.3.1 Computation of the values of magnetic induction produced by the substation 75
4.3.2 Design of the shielding system 79
4.3.3 Result of the simulations 80
4.3.4 Conclusion 85

4.4 Shielding of a typical MV/LV substation of the local distributor 86
4.4.1 Computation of the values of magnetic induction produced by the substation 87
4.4.2 Validation of the sources models 91
4.4.3 Design of the shielding system 98
4.4.4 Result of the simulations 101
4.4.5 Implementation of the shielding system 111
4.4.6 Real test of the shielding system and conclusion 112
4.5 Modular shielding system for MV/LV substations 115
4.5.1 Design of a single part of the shielding system 116
4.5.2 Influence of the connection among slabs 121
4.5.3 Experimental test on a substation prototype 124
4.5.4 Conclusion 132
4.6 Shielding system for a complex substation 133
4.6.1 Base configuration of the MV-LV substation 134
4.6.2 Transposition of the transformers 135
4.6.3 Transposition of cables 136
4.6.4 Multilayer magnetic shielding plates 137
4.6.5 Results of the adopted shielding techniques and conclusion 138
5 Conclusion 139
6 References 145

1 Introduction

Nowadays, the issue of human exposure to electric and magnetic fields is still of worldwide interest [1] [2]. Several institutions investigated this problem trying to define as precisely as possible the effect of the electromagnetic field on the human health. One of the most relevant institution is the International Commission on Non-Ionizing Radiation Protection (ICNIRP) [3]. It is the view of ICNIRP that there is no currently existing scientific evidence that prolonged exposure to electromagnetic field produces possible long-term effect [4], [5]. Therefore, it focused the attention only on the well-established relations between short term direct biophysical effects producing guidelines that suggest the proper limit depending on the field frequency or on the shape of pulsing magnetic field [6] . These limitations are also published in the European Directive 2004/40/EC, [7] that regulates the maximum admissible levels for professional exposures. On the other hand, the protection of population is not homogeneous [2], [8], [9] but, usually a higher degree of safety is introduced considering stricter limits. For the above reasons the emissions of the electrical infrastructures for electricity distributions need to be analyzed. These systems are operated at Extremely Low Frequency (ELF), i.e. 50/60 Hz, therefore, electric and magnetic field can be analyzed separately. It is well known that in the ELF range the possible exceeding of the limit is mainly related to the magnetic field, moreover, the current literature explored quite well the possible mitigation solutions for power lines identifying several options suitable for overhead [10] [11]and underground installations [12] [13] . Finally, it is also important to consider the emission related to the secondary electrical substations. The transformation of medium voltage (MV) in low voltage (LV) by means of a transformer is accompanied by a local increase of the current values on the LV side. Therefore, in the surrounding volume of the substation the magnetic field level is always higher than the average and it is often necessary to employ a mitigation system [14]. The main components of a substation are: MV cables supplying the substation, MV and LV connections between the transformers and the respective MV and LV switchboards, the MV and LV switchboards and MV/LV transformers. Among these components the more crucial, on the magnetic field generation, are the LV connections, the transformer in the case of cast resin transformer and sometimes the LV switchgear. Mitigation of magnetic fields can be done in various ways based on two techniques: optimal displacement of sources and application of screening systems (passive or active). In this elaborate both optimal displacement of sources and application of passive screening systems are take into account.

The first part of the dissertation is devoted to the description of the formulation of the calculation models used to perform the simulations, more particularly are described:

- Calculation models of magnetic field sources
- Models for the simulation of the behavior of various types of shielding materials

The models related to the study of the sources of the field have allowed us to study the various devices that compose the electrical system linking each component to only three types of sources of electromagnetic induction:

- Rectilinear indefinites Conductors (two-dimensional sources)
- Rectilinear finite length Conductors (three-dimensional sources)
- Toroidal Winding

The simulation of the effects of shielding materials is instead based on the finding that the only types of materials that can reduce the values of magnetic induction at low frequency are the materials of conducting type and those of the ferromagnetic type, consequently were elaborated two different types code to simulate the electromagnetic behavior of the two materials.

In particular, the conductive materials are treated by means of the so-called "Low frequency PEEC (partial element equivalent circuit) formulation" [15] [16];

The source code for the ferromagnetic shielding type is instead based on the principle that, in a domain containing ferromagnetic materials sources and the total field is the sum of the contribution of the sources and the perturbation due to the magnetized material [17] [18] .

Finally multilayer shields were treated using a commercial finite element code (FEM) which allowed us to analyze the cases attributable to two-dimensional cases [19].

Once the part concerning modeling, the elaborate proceeds with the description of the set up of the practical tests performed in the laboratory useful to verify the correctness of the results obtained through simulations. More specifically describes in detail the set-up used to test:

- Transformers MV / LV
- MV and LV switchgears
- Power Lines

Special attention is given to the test system on the analysis of the MV / LV transformers since it has been entirely reproduced in the laboratory the set up used to perform typical short circuit tests. The system created allows to test, at their nominal current, transformer size between 100 and 1250 kVA only by absorbing the energy losses due to the power system and the transformer under test. In addition to the description of the power system are reported in the elaborate precautions that have been taken to ensure that the system itself influenced the results of the surveys.

The electrical lines and electrical panels are tested using a transformer specially created and capable of delivering different current values (100 to 1000 A).

The last part of the dissertation is devoted to the description of the study and design of screening systems relating to real case studies. More specifically there are described two application examples for each category of type of analyzed shielding:

- Ferromagnetic Shield
- Conductive Shield
- Multilayer Shield

Within the categories listed above were analyzed cases involving the shielding of areas located in close proximity to high voltage power lines, electrical substations MV/LV, transformers and electrical cabinets with special features.

The elaborate gives also particular emphasis to the different shielding techniques that can be adopted making a distinction between the shielding systems composed of components standard shielding, those specially designed for each component or the specific application to protect only the area involved by high values magnetic induction.

These shielding systems were indeed realized leading to verify the absolute goodness of the calculation models used in the simulations.

In the conclusions is presented an analysis of particular interest relative to the case of a structure positioned below an high voltage power line, for this application it is presented both the study of a fully conductive shielding and a completely ferromagnetic one and the dissertation ends with the description of the strengths and critical points of each solution.

2 Formulation

2.1 Sources

As mentioned in the introduction the evaluation by calculation of the levels of magnetic induction, is of fundamental importance for the study of shielding systems. This chapter describes the models used, which allow to connect the various sources analyzed at only three types of sources of electromagnetic induction:

1) Straight conductors segments carrying currents
2) Toroidal winding
3) Undefined straight Conductors (2D problems)

These 3 models are enough to describe properly all electrical devices of our interest: cables, power lines [20], low voltage switchgear and MV/LV transformers [21]. In particular the first two listed models are useful for the definition of three-dimensional problems (for example, the description of an electrical panel, or a whole substation), the third model is valid for the cases studies that can be traced to two-dimensional problems, such as parallel straight conductors sufficiently long.

Here are then described and analyzed the model of the straight conductor segment and of the toroidal winding.

2.1.1 Straight conductor segment in space:

The calculation model is based on the integration of the Biot-Savart law, through which it is possible to determine at any point in space the value of the magnetic field induction generated by a threadlike conductor traversed by current. In particular, consider a conductor crossed by a current equal to i, such as that shown in Figure 1

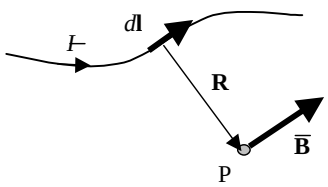

Figure 1 Threadlike conductor traversed by current

This conductor produces in the surrounding space considered homogeneous (air) a magnetic flux density B given by the integral:

$$\overline{\mathbf{B}} = \mu_0 \int \frac{\bar{I} d\mathbf{l} \times \mathbf{R}}{4\pi R^3} \qquad (1)$$

in which:

• dl is an infinitesimal length vector, tangent to the conductor and oriented in the direction of the current

• R is a distance vector between the point on the conductor and the point P in which is to be determined the field

• μ_0 is the absolute permeability (assumed for air) equal to $4\ \pi\ 10^{-7}$

We are interested only in straight conductor segments, so is possible to simplify the general relationship just expressed. Is possible then to calculate the magnetic flux density generated by the current that runs through a straight conductor segment, defined by two points P_1 (x_1, y_1, z_1) and P_2 (x_2, y_2, z_2). It is assumed that the current is directed from P_1 to P_2.

The magnetic induction at a point Q (x_Q, y_Q, z_Q) is equal to:

$$\mathbf{B}(Q) = \mu_0 \int_{P_1}^{P_2} \frac{i}{4\pi} \cdot \frac{\mathbf{dl} \times R}{R^3} \qquad (2)$$

With:

$$\mathbf{dl} = dx\mathbf{a}_x + dy\mathbf{a}_y + dz\mathbf{a}_z \qquad (3)$$

$$R = (x_Q - x)\mathbf{a}_x + (y_Q - y)\mathbf{a}_y + (z_Q - z)\mathbf{a}_z \qquad (4)$$

Is parameterized a straight line using the following parametric expression, the parameter t:

$$\begin{cases} x = x_1 + (x_2 - x_1)t \\ y = y_1 + (y_2 - y_1)t \\ z = z_1 + (z_2 - z_1)t \end{cases} \qquad (5)$$

The outer product of dl x R and the distance R3 of the equation (2) are therefore equal to:

$$\mathbf{dl} \times R = dt(k_x\mathbf{a}_x + k_y\mathbf{a}_y + k_z\mathbf{a}_z) \qquad (6)$$

$$R^3 = \left(at^2 - bt + c\right)^{\frac{3}{2}} \qquad (7)$$

In which the coefficient are:

$$\begin{cases} k_x = y_1\left(z_2 - z_Q\right) + y_2\left(z_Q - z_1\right) + y_Q\left(z_1 - z_2\right) \\ k_y = -x_1\left(z_2 - z_Q\right) - x_2\left(z_Q - z_1\right) - x_Q\left(z_1 - z_2\right) \\ k_z = x_1\left(y_2 - y_Q\right) + x_2\left(y_Q - y_1\right) + x_Q\left(y_1 - y_2\right) \end{cases} \qquad (8)$$

$$\begin{cases} a = \left(x_1 - x_2\right)^2 + \left(y_1 - y_2\right)^2 + \left(z_1 - z_2\right)^2 \\ b = 2\left[\left(x_1 - x_2\right)\left(x_1 - x_Q\right) + \left(y_1 - y_2\right)\left(y_1 - y_Q\right) + \left(z_1 - z_2\right)\left(z_1 - z_Q\right)\right] \\ c = \left(x_1 - x_Q\right)^2 + \left(y_1 - y_Q\right)^2 + \left(z_1 - z_Q\right)^2 \end{cases} \qquad (9)$$

The final analitic solutuion used in the modellization is:

$$\mu_0 \int_{P_1}^{P_2} \frac{i}{4\pi} \cdot \frac{\mathbf{dl} \times R}{r^3} = i \cdot 1 \cdot 10^{-7}\left(k_x \mathbf{a_x} + k_y \mathbf{a}_y + k_z \mathbf{a}_z\right) \int_0^1 \frac{dt}{\left(at^2 - bt + c\right)^{\frac{3}{2}}} =$$

$$= i \cdot 1 \cdot 10^{-7}\left(k_x \mathbf{a}_x + k_y \mathbf{a}_y + k_z \mathbf{a}_z\right) \frac{2\left(2at - b\right)}{\left(4ac - b^2\right)\sqrt{at^2 - bt + c}}\Bigg|_0^1 = \qquad (10)$$

$$= i \cdot 1 \cdot 10^{-7}\left(k_x \mathbf{a_x} + k_y \mathbf{a}_y + k_z \mathbf{a}_z\right) \frac{2\left(2a\sqrt{c} - b\sqrt{c} + b\sqrt{a - b + c}\right)}{\sqrt{c}\left(4ac - b^2\right)\sqrt{a - b + c}}$$

This calculation model is valid for values of instantaneous current . However, for plant applications, it is useful the application of the symbolic method, in order to easily deal the sinusoidal currents. This model of calculation, as well as the other two models implemented in software, are still valid also in the case of use of the symbolic method.

2.1.2 Toroidal winding in the space

The model of the toroidal windings in the space is useful for calculating the magnetic flux density produced by the transformers. In particular, this model will be used in the model to calculate the contribution of cast resin transformers, which are not enclosed inside a metal casing that acts as a shield to stray magnetic fields, as in the case of oil-filled transformers, for which they can generate relevant fields.

The proposed model is based on decomposing of the problem of the transformer field in the calculation of the internal and the external field to the core. The magnetic field inside the core of the transformer is connected to the physical and geometrical characteristics of the core itself, and is due to the magnetizing component of the magnetomotive force given by the difference between the ampere-turns of the primary and secondary. In contrast, the external magnetic field is little influenced by the characteristics of the nucleus and the magnetomotive force magnetizing, but depends mainly on the fact that the windings of the primary and secondary are concentric but with different radius. In the model, the presence of the core is neglected and we consider three pairs of windings, the primary and secondary, in which each pair is fed with ampere-turns equal in magnitude and in phase opposition (Figure 2).

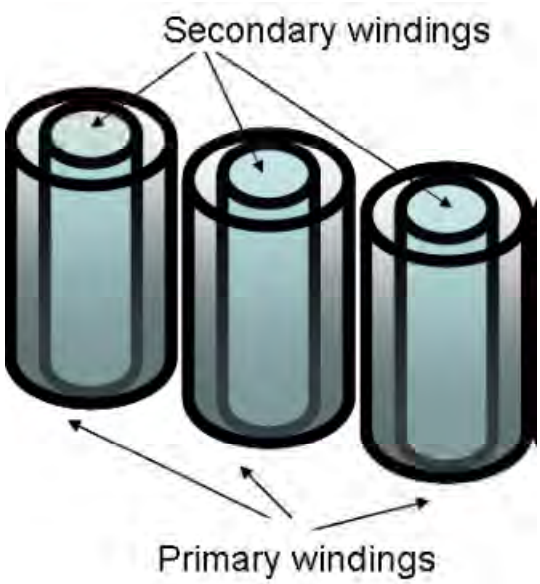

Figure 2 Primary and secondary windings

The calculation model of the transformer is based on the model of a solenoid with rectangular section, for which it requires the use of a reference system in cylindrical coordinates (r, z) because, as the dipole geometry axisymmetric, the poloidal component of the field is identically zero and can be neglected. With reference to Figure 3, the position of the coil is given by the coordinates of the center of the conductor of the coil PS = (r_S, z_S), while the point at which the field is calculated has a coordinate PC = (r_C, z_C).

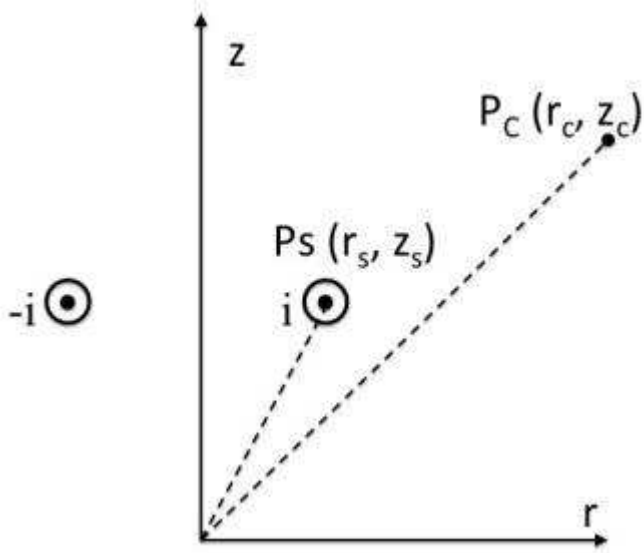

Figure 3 Representation of the circular loop through cylindrical coordinates (r, z)

From the Biot-Savart formula, integrating the curve of the coil, you can get the value of the magnetic field and the magnetic induction at any point in the plane (r_z). The radial (r) and axial (z)expression of the components of the magnetic induction are the following:

$$b_r = i \cdot \frac{\mu_0}{4\pi} \frac{(z_C - z_S)k}{r_C \sqrt{r_C r_S}} \left(-K(k) + \frac{r_S^2 + r_C^2 + (z_C - z_S)^2}{(r_C - r_S)^2 + (z_C - z_S)^2} E(k) \right) = i \cdot f_r(r_S, r_C, z_S, z_C) \qquad (11)$$

$$b_z = i \cdot \frac{\mu_0}{4\pi} \frac{k}{r_C \sqrt{r_C r_S}} \left(K(k) + \frac{r_S^2 - r_C^2 - (z_C - z_S)^2}{(r_C - r_S)^2 + (z_C - z_S)^2} E(k) \right) = i \cdot f_z(r_S, r_C, z_S, z_C) \qquad (12)$$

In which:

- *i* is the current in the filiform coil
- *k* is the argument of elliptic integrals of the first and second type (K and E), defined by:

$$k = \frac{4 r_S r_C}{\left(r_C - r_S\right)^2 + \left(z_C - z_S\right)^2} \tag{13}$$

The elliptic integrals are respectively:

$$K(k) = \int_0^{\frac{\pi}{2}} \frac{1}{\sqrt{1 - k^2 \sin^2 \theta}} d\theta \tag{14}$$

$$E(k) = \int_0^{\frac{\pi}{2}} \sqrt{1 - k^2 \sin^2 \theta} d\theta \tag{15}$$

The relations 11 and 12 allow to calculate the magnetic induction produced by a coil crossed by current in a cylindrical reference system. these formulas are used to calculate the magnetic induction produced by a solenoid with rectangular section. It examines the case represented in Figure 4 , as well it in a reference system in cylindrical coordinates.

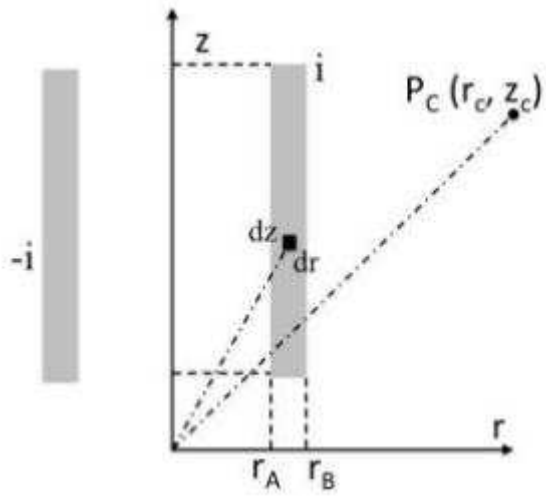

Figure 4 Representation of the solenoid with rectangular cross section through cylindrical coordinates

Assuming that the section is traversed by a uniform current density, which leads to a total current "i", the current density will be equal to:

$$J = \frac{i}{\left(r_B - r_A\right) \cdot \left(z_B - z_A\right)} \tag{16}$$

Considering an infinitesimal surface $ds = dr \cdot dz$ (as shown in Figure 4), according to previous assumptions, it will be crossed by the current $i' = J \cdot dr \cdot dz$, and will consequently that the elementary contributions to the components of magnetic flux density are:

$$db_r = J \cdot drdz \cdot f_r(r_S, r_C, z_S, z_C,) \quad (17)$$

$$db_z = J \cdot drdz \cdot f_z(r_S, r_C, z_S, z_C,) \quad (18)$$

By integrating on the cross section of the solenoid is obtained the total contribution:

$$B_r = \int_{z_A}^{z_B}\int_{r_A}^{r_B} J \cdot f_r(r_S, r_C, z_S, z_C,) \cdot drdz \quad (19)$$

The integral is calculated numerically by using adaptive quadrature formulas that are able to maintain the accuracy of the result uniform regardless of the distance of the calculation point and of the source points inside the solenoid.

The code pattern of the solenoid with rectangular section just described to calculate the magnetic flux density produced by a cast resin transformer, which is modeled using six solenoids rectangular section. Two by two solenoids represent a column of the transformer, as shown in Figure 5. The current density is related to the ampere-turns of the transformer:

$$J_k = N_2 I_k / [(r_B - r_A)(z_B - z_A)] \quad (20)$$

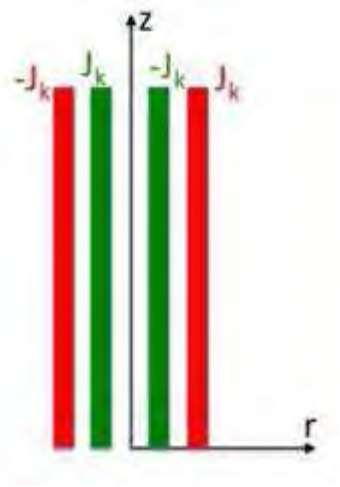

Figure 5 Representation of the column of a transformer by means of two solenoids rectangular section

The total field is obtained by the superposition of effects of the contributions associated with the six solenoids rectangular section that constitute the three columns, taking care to pass from the local reference system of each solenoid (in cylindrical coordinates), to the reference system of the problem in examination (in Cartesian coordinates).

2.2 Application of symbolic method for sinusoidal currents

It 'should be noted that the model calculations described in the previous paragraphs refer to instantaneous value of the current flowing through the wires. However, since all the operators used in the models are linear, and that in all cases of calculation is used the hypothesis of linearity magnetic, it is possible to use these models even with the effective values of currents, and it is also possible to use these models within the symbolic method, in the case where the current used for the calculation are expressed in complex notation (magnitude and phase). In fact, dealing with three-phase systems, it is inevitable to use the symbolic method for the description of sinusoidal currents.

It is important to observe that if the input values are provided as RMS currents, the output will be provided with the RMS value of the magnetic induction (value at which the technical standards and legislative restrictions are refereed).

If however the input it has a current expressed in the real part and imaginary part, the calculation models will be applied separately and independently to the real value and the imaginary value, and the result will again be the real part and the imaginary part of the induction magnetic generated. It has therefore for example that, if the source of the field is a conductor carrying a current expressed in complex notation, for each of the points, which will be calculated in the magnetic flux density, the calculated scalar values will be 6:

1) real component on the x axis
2) imaginary component on the x axis
3) real component on the y axis
4) imaginary component on the y axis
5) real component on the z axis
6) imaginary component on the z axis

For this reason, the data structure in which the code will enter the results of calculation, will be composed of six scalar values n·6, where n is the number of points where it has been carried out the calculation of the magnetic induction.
If the sources are more than one (for example, a three phase conductors), for each point of calculation will be performed the sum for components of the contributions of each individual source. Once added all contributions, the value of magnetic flux density which will be provided in the output, for each of the points in which it was carried out the calculation, will correspond to the scalar module components of the vector to 6 corresponding to that point.

2.2.1 Implementation of the model of the transformer

The model allows to calculate the transformer components Bx By Bz of the magnetic induction produced by the columns of a transformer at each point in space. In order to integrate these algorithms in the numerical code, you must implement procedures making it possible to run the model. In particular, we want to get a calculation function that provides the components Bx By Bz of the magnetic induction generated by the transformer, calculated at any point. This function will input the following data (refer to the diagram of Figure 6):

- N_1: number of coils of medium voltage primary windings (MV)
- N_2: number of turns of low voltage secondary windings (LV)
- D_{MV}: average diameter of medium voltage primary windings (MV)
- D_{LV}: mean diameter of low voltage secondary windings (LV)
- H_{coil}: height of LV and MV windings
- D_{ax} distance of axis winding or axis columns

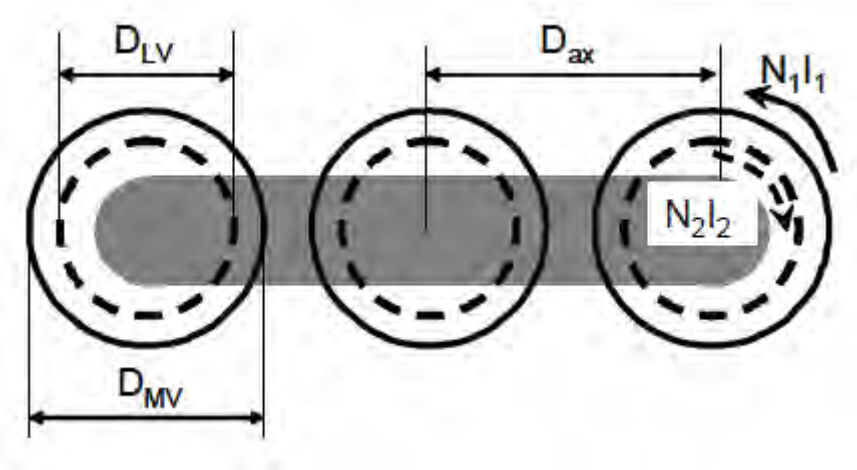

Figure 6 Characteristic geometric parameters for the evaluation of external magnetic fields

It is not immediately find these parameters, since these values are not subject to calculation by the designer of the MV / LV substation, and are not easily be derived from the technical documentation issued by suppliers. However, it should be noted that the distribution transformers are made by all manufacturers with the same design criteria and usually have standard sizes, which depend on the rated power of the transformer. Thus, through the application of classical constructive relations adopted in the regulation of electromechanical constructions, it is possible to have models that allow you to evaluate the external magnetic fields.

Is described below the application of these procedures to compile a table in which, starting from the rating power of the transformer, you can find the values of the structural dimensions that are required for the application of the calculation model of the transformer.

2.2.1.1 Calculation of the core section

From the rated power of the transformer it can be estimated the maximum value of the magnetic flux:

$$\phi = S_{Fe} B \qquad (21)$$

that is related to the power of the transformer and to the design specifications such as the values of exploitation of the materials (B, J). The magnetic flux can be determined using the following relationship:

$$\phi = C_d \sqrt{\frac{S_d}{f}} \qquad (22)$$

With:

- S_d apparent sizing power in kVA
- f frequency in Hz
- C_d coefficient that summarizes the design choices, the values of this coefficent are listed in the Table 1:

	Column Core	Armored Core
Threephase Transformers	$(1 \div 1.6) \cdot 10^{-2}$	$(2 \div 3) \cdot 10^{-2}$
Monophase Transformers	$(1.2 \div 1.9) \cdot 10^{-2}$	$(3 \div 4) \cdot 10^{-2}$

Table 1 Tipical values of C_d for frequency of 50 Hz

Starting from the magnetic flux, we can calculate the rms value of the emf induced in a loop:

$$E_s = 4.44 \Phi_M f \qquad (23)$$

It can be then calculate the number of coils which constitute the primary and secondary winding through the following relations, valid for three-phase transformers Dyn:

$$N_1 = \frac{E_1}{E_s} = \frac{V_1}{E_s} \qquad (24)$$

$$N_2 = \frac{E_2}{E_s} = \frac{V_2}{\sqrt{3}E_s} \qquad (25)$$

In which E indicates the value of the voltage present at the terminals of the winding and V indicates the mains voltage, the number of turns should be approximated to the nearest integer. Assuming that the magnetic circuit is made up of laminations of Fe-Si oriented crystal, are shown Table 2, the typical values of magnetic induction at which they can work

Nominal Power S_d (kVA)	Magnetic induction B (T)
1	1.1 - 1.3
10	1.3 -1.6
100	1.6 – 1.7
1000	1.7 - 1.8
10000	1.8 -1.85

Table 2 Typical values at working point of magnetic induction un the core

Can be calculated the value of the section of the core, and the diameter of the circle that circumscribes it.

$$S_{Fe} = \frac{1}{k_{Fe}} = \frac{\Phi_M}{B} \qquad (26)$$

$$D = \sqrt{\frac{4S_{Fe}}{\pi}} \qquad (27)$$

.

Where K_{FE} is a coefficient taking into account the insulation thickness of the laminations, of the step-wise shape of the nucleus and other surfaces not useful to the conduction of the magnetic flux. We assume that factor equal to: $K_{FE} = 0.85$.

2.2.1.2 Sizing of the windings

For distribution transformers a common practice is to build the secondary winding to slabs of aluminum or copper, while the primary winding (often divided into coils) is constructed with ribbons, plate or wire of aluminum or copper. The height h of the coil that constitutes the winding can be determined by the "linear electrical load of the column", which is an indicator of the exploitation thermal and electrical of the winding and is linked to the power of the transformer. By the laws of similarity, this parameter varies in proportion to the linear dimensions of the machine, which in their turn vary proportionally to the fourth root of the power of dimensioning of the machine. Therefore, this parameter, named "amperewire for cm", is defined as

$$K_{fe} = \frac{N_1 I_1}{h} = \frac{N_2 I_2}{h} = c_k \sqrt{\Phi_M} \qquad (28)$$

Where c_k is a coefficient that takes into account the voltage drop Vdc%, and whose values are shown in the following table:

	c_k
Oil Transformers	2000-2500
Cast resin Transformer	1300-1500

Table 3 Indicative values of the c_k parameter

The considerations are related only to matters magnetic and are valid both for resin transformers both oil, but the different characteristics of insulation and cooling affect the size of the windings. For this reason, the following considerations must be made separately for dry-type transformers and oil transformers. However, we will not analyze the case of oil-filled transformers, because we do not need the size characteristics of these transformers. In fact, the model of the calculation of the magnetic induction generated by the coils of transformers is valid only for the cast transformers, for which there is not a metal casing that acts as a screen. The metal casing of the oil transformer reduce the contribution, at the magnetic induction, of the coils and so his contribution became negligible compared to that of the LV outputs.

2.2.1.3 Self-cooled cast resin transformers

The size which leads to determine the outer diameter of the coils is the overall width of the machine, it can take on that the external dimensions of the coil of MV is 0.31 times the width L of the transformer (0.31 and not 1/3 in order to take into account the space between the coils). Starting from the data regarding the physical dimensions of the commercial cast resin transformers (Easy to find in the technical documentation of the constructor of the transformers), we can obtain the values of:

• Diameter of the core

• Outer diameter of the coil MT

• Average radius of the coils LV and MV

Then it is possible to extract the height of the coils LV and MV, using the equation:

$$h_{bob} = \frac{N_1 I_1}{c_k \sqrt{\Phi_M}} \qquad (29)$$

Where the factor c_k is set equal to 963 instead of the value indicated in 1300, in order to have greater correspondence between the calculated and actual size.

Finally, it is possible to calculate the total size for a cast resin transformer MV / LV, through the following relations:

• Width = (2 * Distance between axles) + Average diameter coil MT

• Depth = 1.8 * Average diameter coil MT

• Height = Height coils + (2 * Column diameter of the nucleus)

Table 4 shows all the values of the characteristic dimensions calculated for each of the values of the nominal power of cast resin transformer MV / LV.

Nominal Power kVA	Number of dipole in the coil	Diameter of the core column	Average diameter of the LV coil	Average diameter of the MV coil	Height of the coil	Distance from the axis of the coils	Width of transform er	Depth of transform er	Height of tranform er
100	49	138	208	263	505	373	1009	473	781
160	39	155	232	294	568	406	1106	529	877
200	35	163	245	310	600	419	1148	558	926
250	31	172	258	327	635	436	1198	588	979
315	28	182	272	345	672	455	1256	621	1036
400	25	192	288	365	714	485	1336	658	1098
500	22	203	304	385	755	502	1388	693	1160
630	20	214	321	406	800	515	1436	732	1227
800	17	226	339	430	849	538	1505	773	1301
1000	16	239	358	454	897	558	1569	817	1375
1250	14	252	378	479	949	584	1647	862	1453
1600	12	268	401	509	1009	607	1723	915	1545
2000	11	283	424	537	1067	640	1817	966	1632
2500	10	299	448	567	1128	680	1927	1021	1726

Table 4 Summary of the characteristic dimensions of cast resin transformers MV / LV

The characteristics size calculated by this procedure were placed in a special database, from which the calculation code takes the input data to be passed to the functions for the calculation of the magnetic induction generated by the cast resin transformers. So, to evaluate the effect of a MV / LV transformer, it is not necessary to specify all its construction data, but it is sufficient to specify the rated power of the transformer.

2.3 Shielding system

The simulation of the effects of shielding materials is instead based on the observation that the only types of materials that can mitigate the values of magnetic induction in the low-frequency materials are conductive and ferromagnetic ones.

In the case of Ferromagnetic material with high magnetic permeability allows the reduction of the magnetic flux density in a shielded area through the flux lines deviation as shown in Figure 7(a) [22] . Usually isotropic or grain oriented ferromagnetic laminations similar to those adopted in the electrical machine industry are used [23].

Conductive materials, the time varying magnetic field produced by AC sources induces eddy currents inside the shield and, consequently, they generate an additional field that modifies and reduces the main magnetic field produced by the sources as shown in Figure 7 (b). Usually, the materials adopted for conductive shields have electrical conductivity higher than 10 MS/m as copper or aluminum; in particular the aluminum is of then preferred for its lower specific weight, which makes possible a significant reductions of weight and cost of the shielding structure.

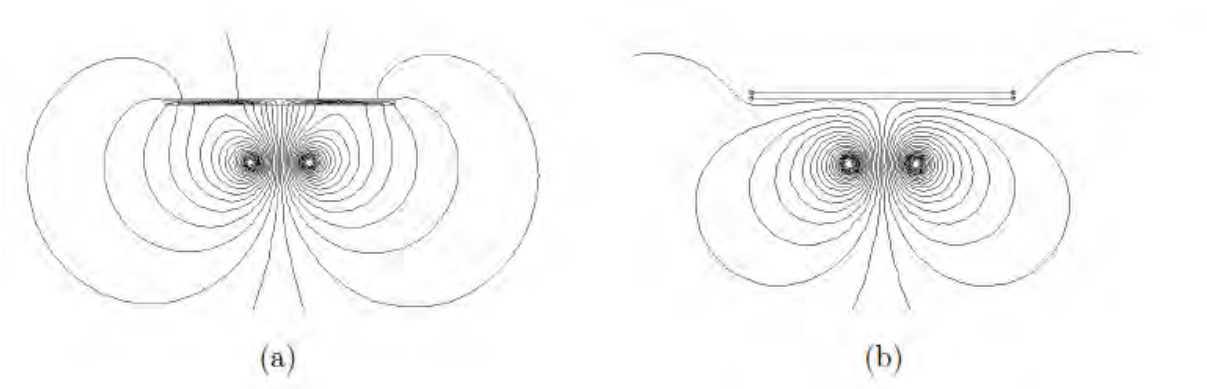

Figure 7 The ferromagnetic material is a low reluctance path for the magnetic field (a) The induced currents inside the conductive shield create an additional field that deviates the source field (b).

Two different types of codes to simulate the electromagnetic behavior of the two materials have been developed.

The model for ferromagnetic shielding type is instead based on the principle that, in a domain containing sources and ferromagnetic materials the total field is the sum of the contribution of the sources and the perturbation due to the magnetized material [17] [18] [24] .

The conductive materials are treated using the so-called "Low frequency PEEC (partial element equivalent circuit) formulation" [15] [16] ;

2.3.1 Ferromagnetic Materials

Regarding ferromagnetic materials the overall magnetic field is

$$\boldsymbol{H} = \boldsymbol{H}_s + \boldsymbol{H}_m \quad (30)$$

being Hs is the magnetic field generated by the sources (e.g. conductors and transformers), and Hm is the demagnetizing field generated by the magnetization M inside the ferromagnetic bodies.

Open shields often works far from saturation levels, therefore the overall magnetic field H can be assumed linearly dependent on the magnetization M. Therefore M = χ H, being χ the magnetic susceptibility. Moreover, the demagnetizing field is related to the magnetization by means of the demagnetizing tensor N:

$$\boldsymbol{H}_m = -\boldsymbol{NM} \quad (31)$$

The combination of the previous equations makes it possible to define a single relation that links the magnetization to the external field:

$$\frac{\boldsymbol{M}}{\chi} + \boldsymbol{NM} = \boldsymbol{Hs} \quad (32)$$

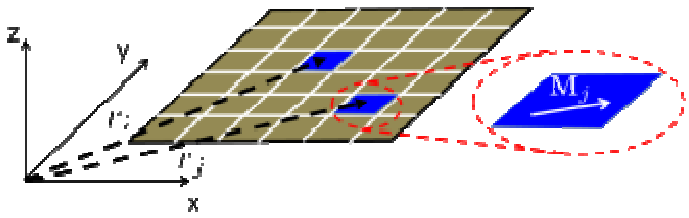

Figure 8- The shield is discretized in several surface elements. The magnetization becomes a discrete distribution and each element is characterized by a constant magnetization value

Eq. (32) is used together with a surface discretization of the shield as shown in Figure 8, here the magnetization becomes a discrete distribution and each element is characterized by a constant magnetization value. If eq. (32) is written at the barycenter of each element (rectangular block) of the shield, a linear system of equations is found with the magnetization M as the only unknown. Once the magnetization M is obtained, the demagnetizing field can be evaluated and used for the computation of the overall magnetic field as reported below:

The equations 31 and 32 written at the barycenter of each element i become respectively the eq. (33) and (34).

$$H_{mi} = -\sum_j N(r_i - r_j)M_j \qquad (33)$$

$$H_{si} = \frac{M_i}{\chi} + \sum_j N(r_i - r_j)M_j \qquad (34)$$

Solution of (34) provides magnetizations Mi and the whole magnetic field can be eventually calculated at each point inside the shield.

By using (33) for the magnetostatic field and superposing it to applied field in (32). The computation of magnetic field at any external point can be also obtained for a known M distribution. A solution of the linear system (34) can be obtained by a direct method. But since the system has a full matrix, its computational complexity is of order 0(n3), n being the number of unknowns.

2.3.2 Conductive Materials

An integral approach to Maxwell equation for the modeling of interconnects and packaging structures are usually preferred to differential ones because they allows to solve the field equations in term of sources of field located on the metallic structures.

Among the various techniques integrals, the PEEC method allows to describe the electromagnetic problems in terms of circuit parameters that represent the magnetic and electric coupling between the current and the charge of the discrete structure.

In this elaborate a generalized PEEC methodology have been applied by the use of the topological concept of duality [25].

This method ensures the correct formalization of the PEEC tessellation but also allows manipulate the mesh general, both structured and unstructured. This is very important since it allows the use of triangular meshes only if necessary (ie, curved or slanting electrodes), leaving in the regular regions, the orthogonal discretization, with an overall improvement of computational performance.

For this method it is really important to make the dual disccretization in a correct way [26] [27]. Some general information about the dual discretization are reported in the next sub-chapter.

2.3.2.1 The dual discretization

A reformulation of field laws in a direct finite formulation must start with an analysis of physical quantities in order to make explicit the maximum of information content that is implicit in definition and in measurement of physical quantities. To this end it is convenient to introduce two classifications of physical quantities.

A first classification criterion of great usefulness in teaching and in research is that based on the role that every physical variable plays in a theory. Analysis of the role of physical variables in a theory leads to three classes of variables:

- Configuration Variable
- Source Variable
- Energy variable

These three classes for electromagnetism are shown in Figure 9.

The configuration variable describe the configuration of the field or system and are linked to one another by operations of sum, difference, limit, derivative and integral. They are linked to the source ones by the constitutive equations.

The source variable describe the sources of the field or the forces acting on the system and are linked one to one another by operations of sum, difference, limit, derivative and integral.

The product of a configuration and a source variable provide an Energy variables; even the energy variable are linked to one another by operations of sum and difference, of limit, of derivative and integration.

This classification has a central role in physical theories and allows constitutive equations to be defined as Equations linking configuration with source variables and which contain material and system parameters.

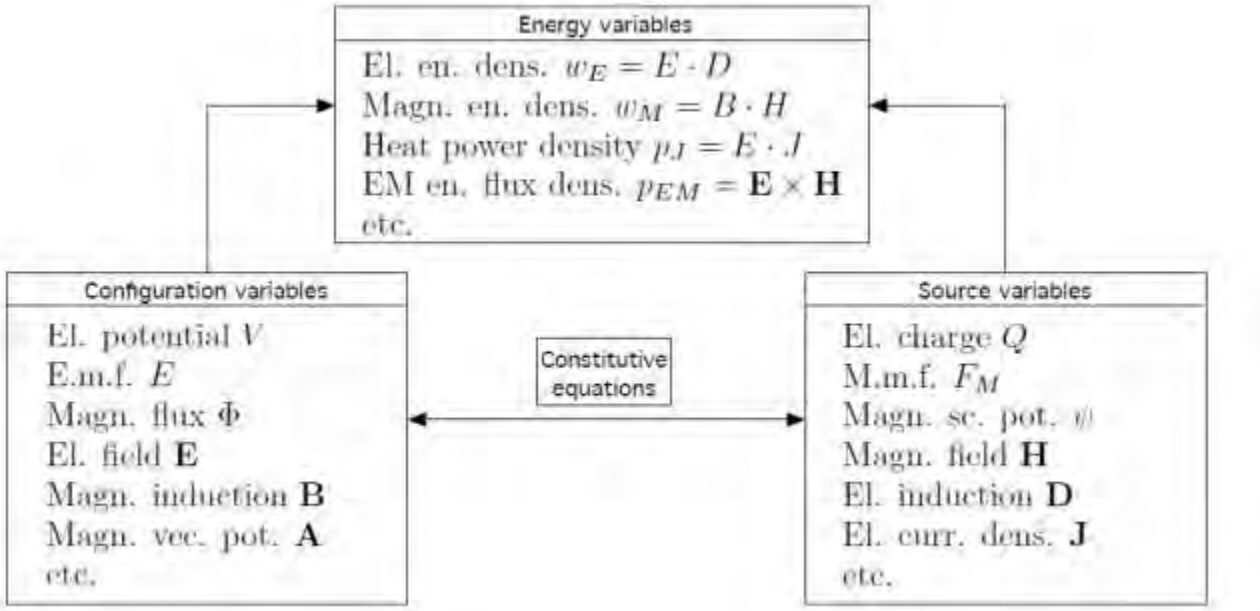

Figure 9 Scheme of links between the different variables

Another important topic that is to be introduced is the link between physical variables and geometry. There is a strict link between physics and geometry and global physical variables are naturally associated with space and time elements, i.e. points, lines, surfaces, volumes, instants and intervals. In order to examine such association we need the notion of orientation of a space element.

In differential formulation a fundamental role is played by points: field functions are point functions. In order to associate points with numbers we introduce a coordinate systems.

In finite formulation we need to consider not only points (P) but also lines (L), surfaces (S) and volumes (V). We shall call these space elements. The natural substitute of coordinate systems are cell complexes. They exhibit vertices, edges, faces and cells. The latter are representative of the four spatial elements P,L, S,V.

The notions of inner and outer orientation of a space element play an important role in electromagnetism as well as in all physical theories. The two notions of inner and outer orientations in three-dimensional space are presented in Figure 10.

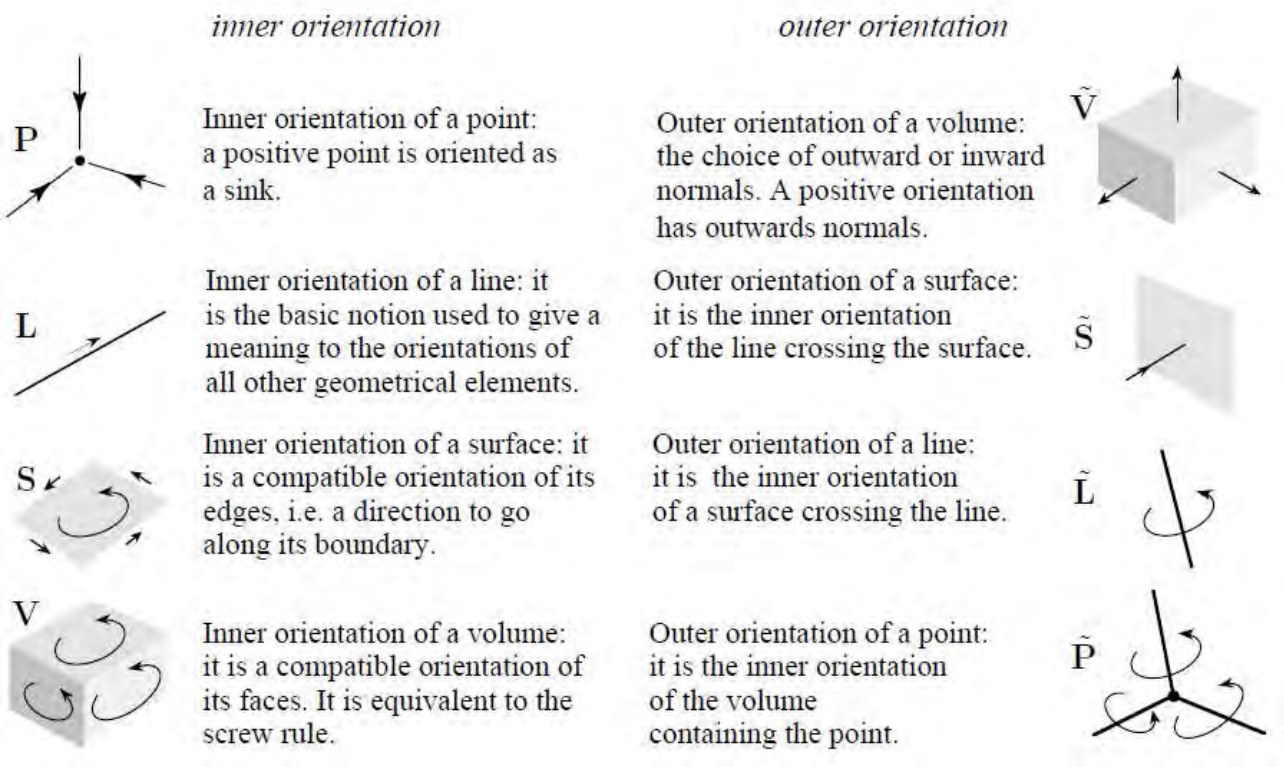

Figure 10 notions of inner and outer orientations in three-dimensional space

- *Inner orientation*. We shall refer to Figure 10, points can be oriented as "sources" or "sinks". The notion of source and sink, borrowed from fluid dynamics, can be used to define an inner orientation of points because it permits us to maintain the notion of incidence number from lines and points. In particular we note that points are usually oriented as sinks. This is never explicitly stated but it can be inferred from the fact that space differences of a point function between two points P and Q are given by (+1)f(Q) + (−1)f(P). This means that the line segment PQ, oriented from P to Q, is positively incident in Q (incidence number +1) and negatively incident in P (incidence number −1). In other words: in the expression (Q−P) signs can be interpreted as incidence numbers between the orientation of the line segment and those of its terminal points. A line is endowed of inner orientation when a direction has been chosen on the line. A surface is endowed with inner orientation when its boundary has an inner orientation. A volume is endowed with inner when its boundary is so.

- *Outer orientation*: To write a balance we need a notion of exterior of a volume, because we speak of charge contained in the volume. This is usually done by fixing out wards or

inwards normal to its boundary, as shown in Figure 10 (right). A surface is equipped with outer orientation when one of its faces has been chosen as positive and the other negative: this is equivalent to fixing the direction of an arrow crossing the surface from the negative to the positive face, as shown in Figure 10 (right). We need the outer orientation of a surface when we consider a flow crossing the surface. A line is endowed with outer orientation when a direction of rotation around the line has been defined: think to the rotation of the plane of polarization of a light beam. A point is endowed with outer orientation when all line segment with origin in the point have an outer orientation. Think, for example, to the sign of the scalar magnetic potential of a coil at a point: its sign depends on the direction of the current in the coil. The four space elements endowed with outer orientation will be denoted $\widetilde{P}\,\widetilde{L}\,\widetilde{S}\,\widetilde{V}$. Contrary to inner orientation, outer orientation depends on the dimension of the space in which the element is embedded, as shown in Figure 11. Hence exterior orientation of a line segment embedded in a three-dimensional space is a direction of rotation around the segment; in a two-dimensional space it is an arrow that crosses the line and when the segment is embedded in a one-dimensional space, it is represented by two arrows as if the segment were compressed or extended.

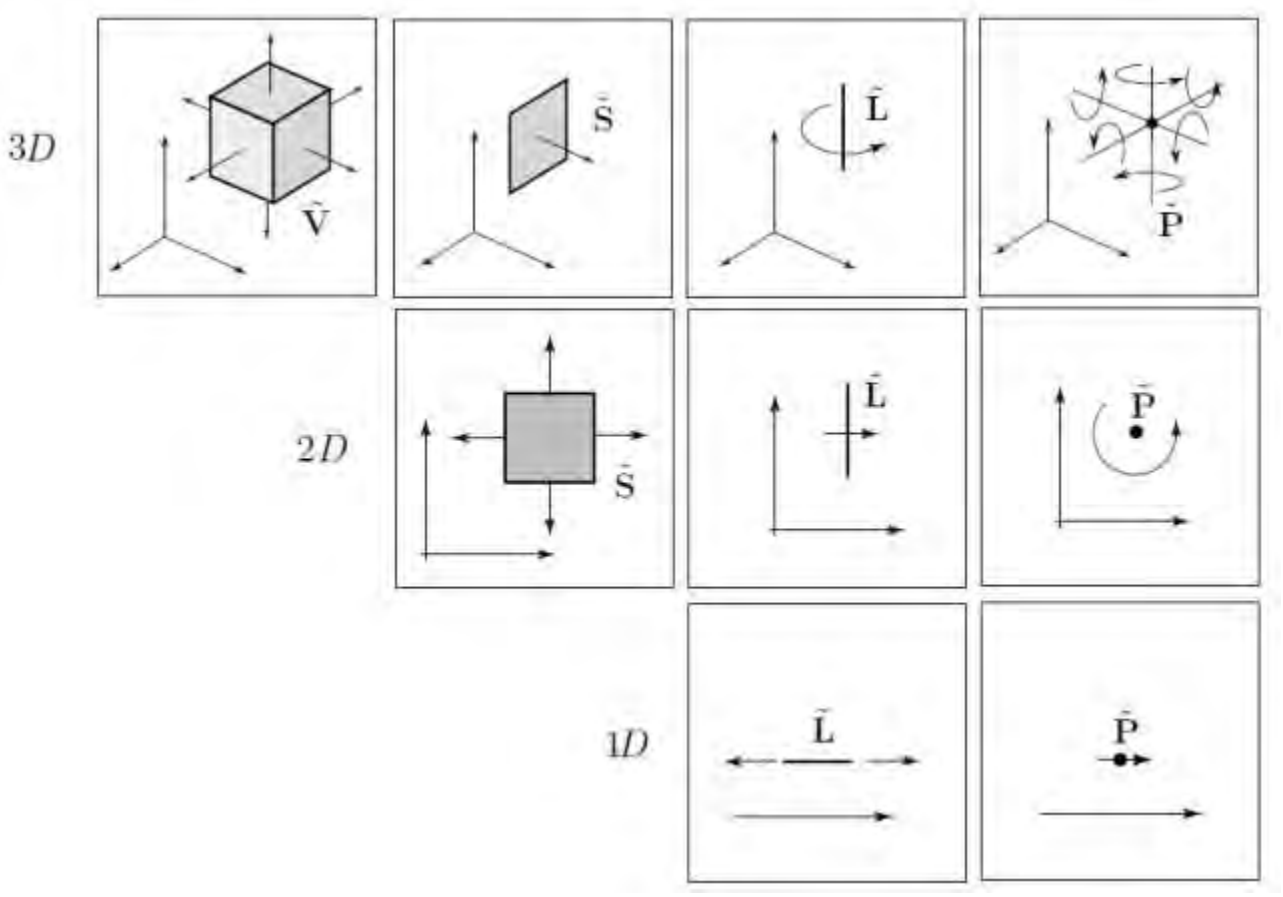

Figure 11 The outer orientation of a space element depends on the dimensions of the embeddingspace.

All the information described in this section are useful to understand how the problem is solved. The principle is a bit complex: we build up a cell complex in the region in which the field is considered and then apply the equations in finite form to all cells of the complex. Some equations must be applied to the cells others to their faces; some equations must be applied to the cells and faces of the primal, some other to those of the dual complex. Doing so we obtain a system of algebraic equations whose solution gives the space and time distribution of the global variables of the field. In this way we solve the fundamental problem of electromagnetism: given the space and time distribution of charges and currents to find the resulting field. Some example of cell complex is presented in Figure 12

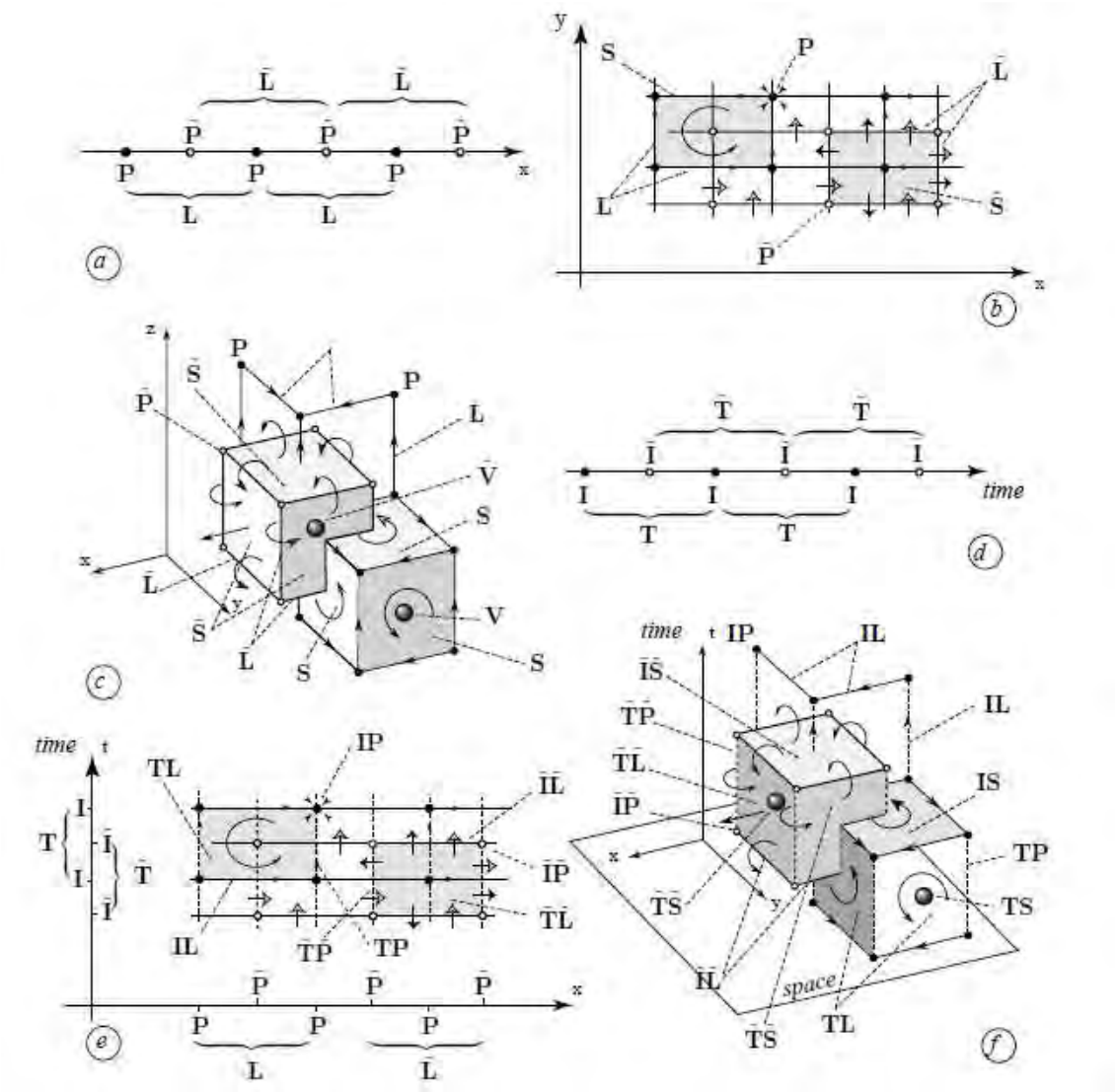

Figure 12 (a) A one-dimensional cell complex; (b) a two-dimensional cell complex; (c) a three-dimensional cell complex; (d) a one-dimensional cell complex on a time axis; (e) a cell complex in two-dimensional space-time; (f) a cell complex in three-dimensional spacetime.

A cell complex can be based on a coordinate system: in such a case the edges of the cells lie on the coordinate lines and the faces on the coordinate surfaces. An example is shown in Figure 14 (left) . A coordinate-based cell complex is useful when one aims to deduce the differential formulation from a finite one.

Conversely, for numerical applications it is convenient to give up the coordinate based cell complex and to use simplicial complexes, i.e. the ones formed by triangles in 2D and tetrahedra in 3D. Simplicial complex have many advantages over the coordinate-based complexes. A first advantage is that simplexes can be adapted to the boundary of the domain, as shown in Figure 13 .

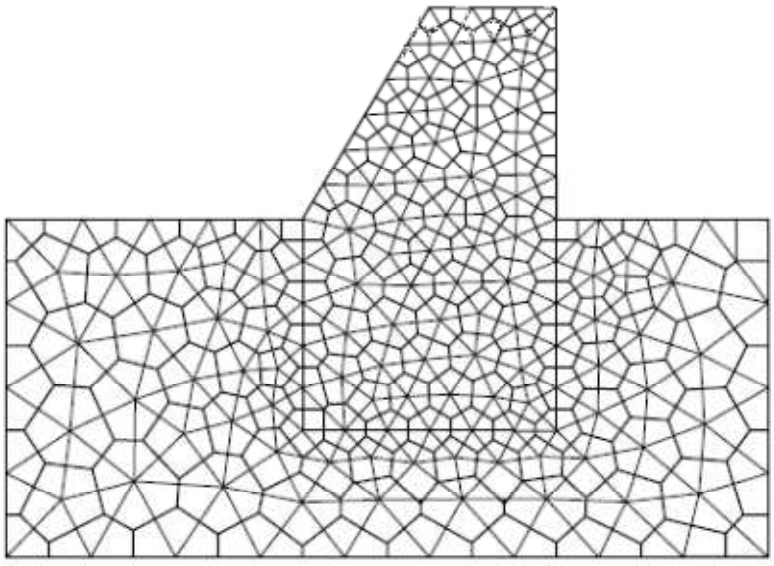

Figure 13 Finite formulation permits different materials to be treated assuringcon tinuity at the separation surface automatically.

A second advantage is that, when we have two or more subregions that contain different materials, the vertices of the simplexes can be put on the separation surface, as shown in Figure 13. A third reason is that simplexes can change in size from one region to another. This allows to adopt smaller simplexes in the regions of large variations of the field. Once we have introduced a cell complex we can consider the dual complex. In a coordinated-based complex one can consider the barycenter of every coordinate-cell as shown in Fig. 9. Connecting the barycentres of the adjacent cells one obtains a dual complex. The term "dual" refers to the fact that not only every barycenter (dual vertex) corresponds to a cell (primal volume) but also every edge of the dual complex (dual edge) intersects a face of the primal one (primal face). Conversely, every primal edge intersects a dual face. Lastly, every vertex of the primal lies inside a cell of the dual.

An example of dual cell complex is presented in Figure 14.

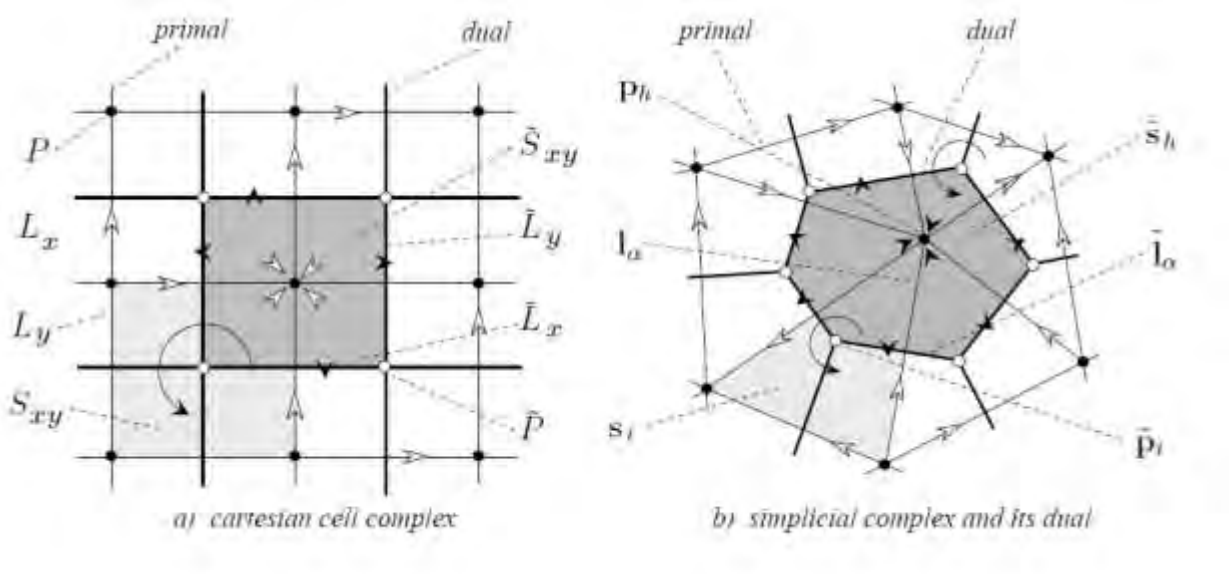

Figure 14 two-dimensional cell complex (thin lines) and its dual (thick lines)

A cell complex and its dual enjoy a peculiar property: once the vertices, edges, faces and cells of the primal complex has been endowed with inner orientation, this inner orientation induces an outer orientation on the cells, faces, edges and vertices of its dual. It follows that a pair formed by a cell complex and its dual are the natural frames to exhibit all space elements with the two kind of orientations. Since we have stated that the configuration variables are associated with the space elements endowed with inner orientation, it follows that the configuration variables can be associated with the vertices, edges, faces and cells of the primal complex. Moreover since the source and energy variables are associated with space elements endowed with outer orientation, it follows that these variables can be associated with cells, faces, edges and vertices of the dual complex. One can say that the role of the dual complex is to form a background structure to which source and energy variables can be referred.

Table 5 reports the spatial assignment of the variables used in PEEC modeling: scalar potentials are assigned to primal nodes, voltage drops to primal edges, currents to dual faces and charges to dual volumes.

Type	Variable	Spatial Element
Source	Current ,i	Dual Face, $\bar{\Sigma}$
	Charge, q	Dual Volume, $\bar{\Omega}$
Configuration	Voltage drop ,u	Primal Edge , λ
	Scalar Potential , φ	Primal Node *P*

Table 5 Spatial assignement of the variable used in PEEC modelling

This definition of duality relations of grids and the rigorous assignment of physical variables to spatial entities allows the possibility of giving a general framework of PEEC modeling, i.e., allowing the use of unstructured and mixed structured/unstructured complexes of cells.

Making reference to Figure 15 the discretization of conductors is made by prisms with triangular or rectangular basis. This tessellation constitutes the dual complex of cells. The primal complex is obtained by connecting the centroids of dual volumes by piecewise segments crossing the lateral faces of prisms.

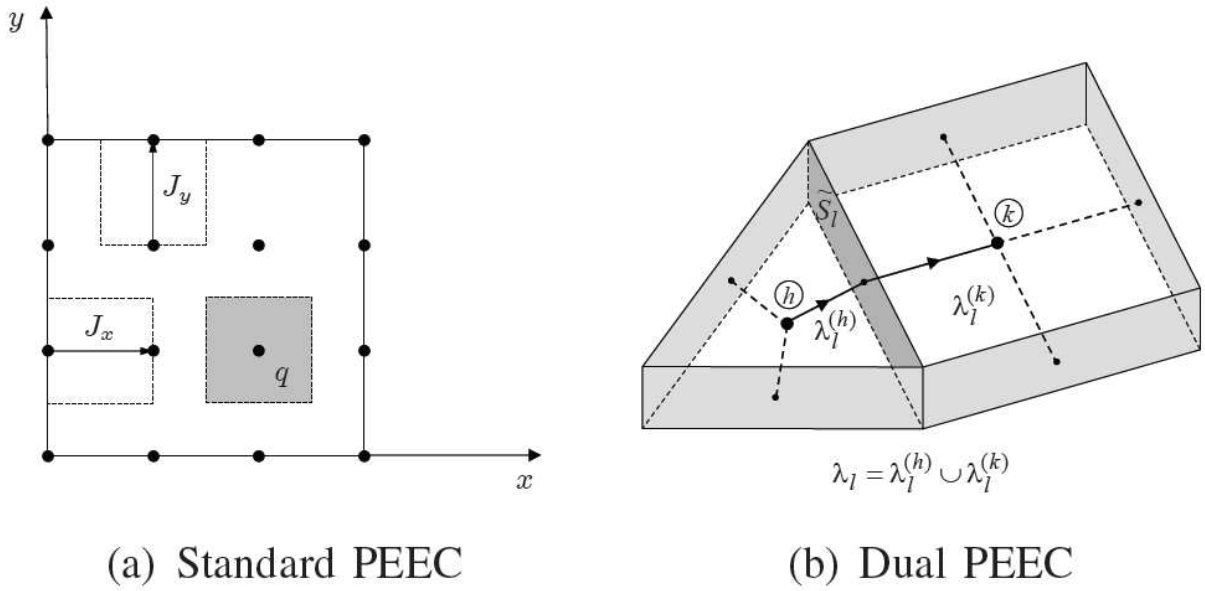

Figure 15 (a) Standard 2D discretization of current density (dashed cells) and charge density (gray cell), (b) dual discretization: the couple primal edge (straight line)/dual face (dark gray) correspond to a two terminal circuit component.

After this short introduction on the description of the technique of discretization of the shield, you can switch to the description of the mathematical formulation.

2.3.2.2 Mathematical formulation

The original PEEC formulation is based on the circuit interpretation of the terms of the Mixed Potential Integral Equation (MPIE):

$$\frac{\vec{J}(\vec{r},t)}{\sigma}+\frac{d\vec{A}(\vec{r},t)}{dt}+\nabla\varphi(\vec{r},t)=0 \qquad (35)$$

A and φ are the retarded magnetic vector and electric scalar potential, respectively,

$$\vec{A}(\vec{r},t) = \frac{\mu}{4\pi}\int_{\Omega}\frac{\vec{J}(\vec{r}',t')}{|\vec{r}-\vec{r}'|}d\Omega \qquad (36)$$

$$\varphi(\vec{r},t) = \frac{1}{4\pi\varepsilon}\int_{\Omega}\frac{p(\vec{r}',t')}{|\vec{r}-\vec{r}'|}d\Omega \qquad (37)$$

$$t' = t - \frac{|\vec{r}-r'|}{c} \qquad (38)$$

The solution of the electromagnetic problem is achieved by discretizing equation (35) on the system of surface cells shown in Figure 15 (a). Current and charge densities are expanded in terms of piecewise constant pulse functions.

- Partial self and mutual inductances between nodes, representing the magnetic field couplings;
- Resistive terms between nodes, representing the Joule losses in the conductive material;
- Coefficients of potential at each node, representing the electric field couplings.

When using a general approach to PEEC models, a local interpolation inside dual volumes linking the current density $\vec{J}$ in equation (35) to the global variable i through dual faces is needed . By

referring to the generic dual volume or cell k identified by a prism of thickness δ_k, and assuming a uniform $\vec{J}$ distribution over the electrode thickness, facet elements basis functions $\vec{\omega}$ are chosen,

$$\vec{J}_k = \frac{1}{\delta_k} \sum_{m=1}^{N_F} i_{km} \vec{\omega}_{km} \quad (39)$$

Where N_F is the number of dual faces in each cell (3 or 4 in our case), i_{km} is the current through the mth dual face of cell k. Many choices for $\vec{\omega}$ are possible but divconforming basis functions must be selected for edges belonging to triangles, rectangles or common between them. With reference to a local frame (*u; v; ω*) (Figure 16 (a)) the following facet functions for triangles are selected

$$\vec{\omega}_k^3(u,v) = N_j(u,v)\nabla N_i(u,v) \times \vec{n} - N_i(u,v)\nabla N_j(u,v) \times \vec{n} \quad (40)$$

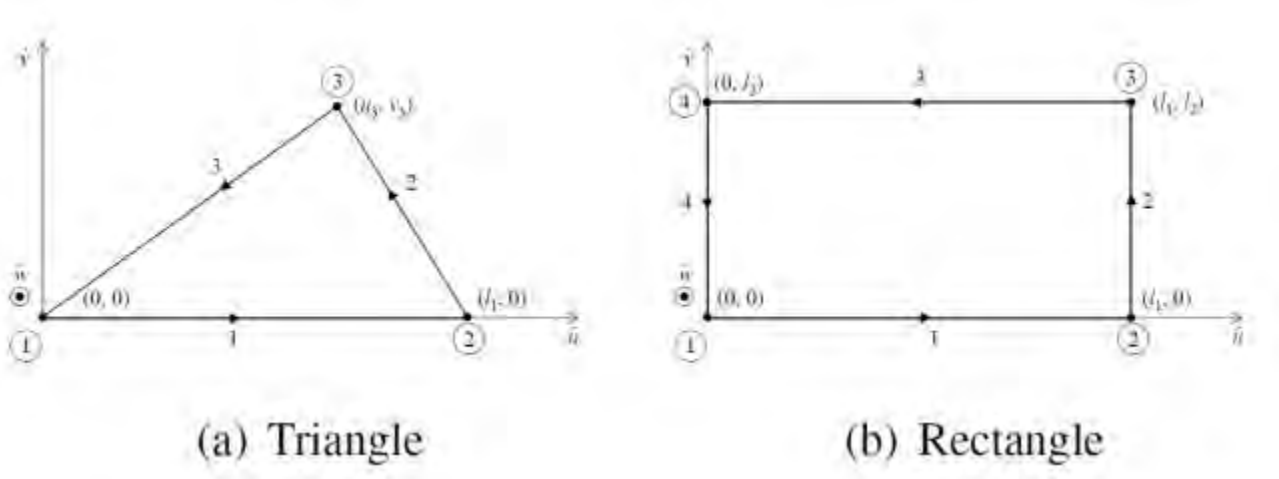

Figure 16 Plane triangle and rectangle in local frame (u; v;w).

where the functions N_i(u; v) and N_j(u; v) are the standard nodal functions related to the extreme nodes of edge k and $\vec{n} = \hat{\omega}$ is the unit vector orthogonal to the triangle surface. The analytical expression of these shape is:

$$\vec{\omega}_1^3(u,v) = \frac{u-u_3}{l_1 v_3}\hat{u} + \frac{v-v_3}{l_1 v_3}\hat{v}$$

$$\vec{\omega}_2^3(u,v) = \frac{u}{l_1 v_3}\hat{u} + \frac{v}{l_1 v_3}\hat{v}$$

$$\vec{\omega}_3^3(u,v) = \frac{u-l_1}{l_1 v_3}\hat{u} + \frac{v}{l_1 v_3}\hat{v}$$

For rectangular cells, special basis functions are built with the same properties of the ones for triangles. $\vec{\omega}_k^4$ has only the component orthogonal to edge k and its magnitude linearly decrease from edge k to the opposite one. The analytic expression in the local (*u; v; ω*) coordinate system is,

$$\vec{\omega}_1^4(u,v) = \frac{v - l_2}{l_1 l_2}\hat{v}$$

$$\vec{\omega}_2^4(u,v) = \frac{u}{l_1 l_2}\hat{u}$$

$$\vec{\omega}_3^4(u,v) = \frac{v}{l_1 l_2}\hat{v}$$

$$\vec{\omega}_4^4(u,v) = \frac{u - l_1}{l_1 l_2}\hat{v}$$

It is easy to prove the continuity of the normal component of $\vec{\omega}$ also for common edges shared by rectangles and triangles. These basis functions have the property of being affine with respect to the *u*, *v* coordinates. This fact allows the possibility of using analytical formulas to solve the surface integrals described in the next paragraph . The surface charge density is expanded in terms of piecewise constant functions on each triangular/rectangular cell.

2.3.2.3 Partial Element Calculation

The parameter extraction can be done by following the same rationale of the original PEEC formulation, i.e., testing MPIE equation (35) with the same basis function used to expand current and charge densities. An equivalent approach is here proposed, by making reference to energetic considerations.

- Extraction of the resistances:

The extraction of the resistances start from the formulation of the joule power losses reported below for a generic kth cell:

$$P_k = \int_{\Omega_k} \frac{J_k^2}{\sigma} d\Omega_\mathrm{k} = \frac{1}{\delta_\mathrm{k}^2 \sigma} \int_{\Omega_k} \left(\sum_{n=1}^{N_F} i_{kn}\vec{\omega}_{kn}\right) \cdot \left(\sum_{m=1}^{N_F} i_{km}\vec{\omega}_{km}\right) \cdot d\Omega_\mathrm{k} \quad (41)$$

When only surface approximations are taken into account, the volume integral can be rearranged into a surface one

$$P_k = \frac{1}{\delta_k \sigma} \int_{\Sigma_k} \left(\sum_{n=1}^{N_F} i_{kn} \vec{\omega}_{kn}\right) \cdot \left(\sum_{m=1}^{N_F} i_{km} \vec{\omega}_{km}\right) \cdot d\Sigma_k \quad (42)$$

The power related to the current flowing through the generic αth dual face of cell k is,

$$P_{k\alpha} = i_{k\alpha} \sum_{m=1}^{N_F} \frac{i_{km}}{\delta_k \sigma} \int_{\Sigma_k} \vec{\omega}_{k\alpha} \cdot \vec{\omega}_{km} \cdot d\Sigma_k = i_{k\alpha} \cdot u_{k\alpha} \quad (43)$$

Where

$$u_{k\alpha} = \sum_{m=1}^{N_F} \frac{i_{km}}{\delta_k \sigma} \int_{\Sigma_k} \vec{\omega}_{k\alpha} \cdot \vec{\omega}_{km} \cdot d\Sigma_k = \sum_{m=1}^{N_F} R_{km} i_{km} \quad (44)$$

Then

$$R_{km} = \frac{1}{\delta_k \sigma} \int_{\Sigma_k} \vec{\omega}_{k\alpha} \cdot \vec{\omega}_{km} \cdot d\Sigma_k \quad (45)$$

The voltage drop over half primal edge α depends on currents through all dual faces of cell k.

- Extraction of partial inductances:

Resorting to magnetic vector potential defined in equation (36), the magnetic energy associated to kth cell is:

$$W_k = \frac{1}{2} \int_{\Omega_k} \vec{J}_k \cdot \vec{A} d\Omega_k = \frac{1}{2} \frac{\mu_0}{4\pi} \int_{\Omega_k} \vec{J}_k \cdot \int_{\Omega_k} \sum_{h=1}^{N_{\bar{V}}} \frac{\vec{J}_h}{|\vec{r} - \vec{r}\prime|} d\Omega_h d\Omega_k \quad (46)$$

Where $N_{\bar{V}}$ is the number of dual volumes. By using the expansion equation (39) and extracting only the magnetic coupling between the current α of the kth cell, and current β of cell h, one has,

$$W_{k\alpha,h\beta} = \frac{1}{2} \frac{\mu_0}{4\pi} \int_{\Omega_k} \frac{i_{k\alpha} \vec{\omega}_{k\alpha}}{\delta_k} \cdot \int_{\Omega_k} \frac{i_{h\beta} \vec{\omega}_{h\beta}}{\delta_k |\vec{r} - \vec{r}\prime|} d\Omega_h d\Omega_k \quad (47)$$

Finally, when considering surface complex of cells only, the partial inductance is,

$$L_{k\alpha,h\beta} = \frac{1}{2} L_{k\alpha,h\beta} i_{k\alpha} i_{k\beta} \quad (48)$$

$$L_{k\alpha,h\beta} = \frac{\mu_0}{4\pi} \int_{\Sigma_k} \vec{\omega}_{k\alpha} \cdot \int_{\Sigma_k} \frac{\vec{\omega}_{h\beta}}{|\vec{r} - \vec{r}\prime|} d\Sigma_h d\Sigma_k \quad (49)$$

2.3.2.4 Equivalent Circuit

Figure 17 shows the resulting two terminal component obtained by assembling all the previous contributions, and it is representative of the basic topological structure primal edge/dual face presented in Figure 15 (b). The unstructured PEEC two terminal components can be assembled to obtain the MNA matrix to be solved by a general purpose SPICE-like network simulator. With respect to standard PEEC model, the use of unstructured meshes introduces a local resistive mutual coupling. The use of dependent current sources allows to deal with this problem without increasing significantly the complexity of the circuit.

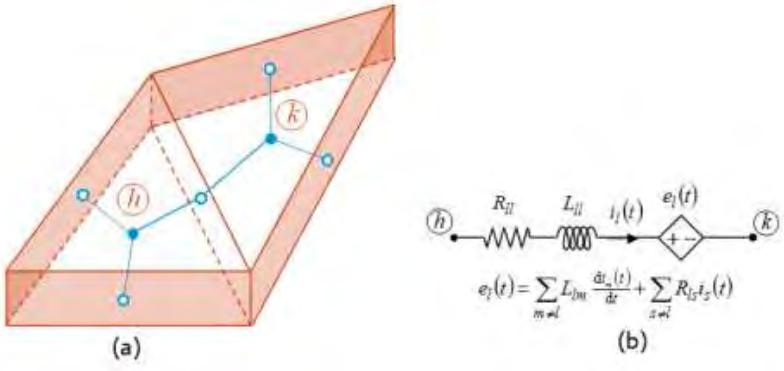

Figure 17 Elementary branch of the PEEC Model

Figure 18 outlines the sequence of necessary steps for the application of dual-PEEC methodology to the solution of a full Maxwell problem. It is worth noting that the added complexity of the method due to the generation of the dual complex and the definition of basis function is negligible with respect to standard technique.

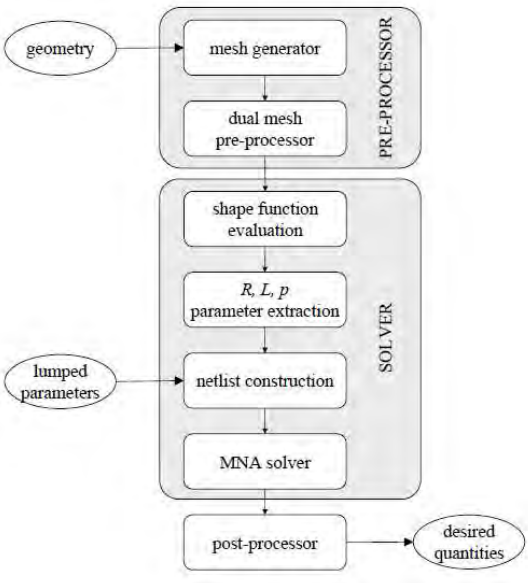

Figure 18 Solver Structure

As far as a low frequency problem is concerned, the typical capacitive term of PEEC formulation is missing.

Equations (49) present a double surface integral, having the Green's function as kernel (in some cases multiplied by an affine combination of the (u; v) coordinates). To speed up the effort of the partial element computation, the inner integrals of equations (49) are solved by analytical formulas. The outer integral is solved by using adaptive Gauss-Kronrod quadrature rule. The number of quadrature points is automatically chosen depending on the distance between cells: the larger the distance, the smaller the number of points needed to reach the convergence of the quadrature rule. Moreover, the computational time for the evaluation of inductance and coefficient of potential matrices can be reduced by considering that these matrices must be symmetric. The standard PEEC formulation can be found as a particular case of the dual formulation when both charge and current densities are expanded in terms of piecewise constant pulse functions. The resulting dual-PEEC circuit is similar to the standard PEEC model, with the exception of a local resistive coupling due to the use of unstructured meshes. The use of current controlled voltage sources allows to deal with this problem with a negligible computational effort (see Figure 17 (b)). In frequency domain the inclusion of retardation is straightforward and makes PEEC equivalent to a full wave solution of Maxwell's equations. It can be done by multiplying the non retarded mutual inductances and coefficients of potential by $\exp(-j\omega\tau_{hk})$, where τ_{hk} is the delay time between the center coordinates of primal edges and dual volumes, respectively.

2.3.3 Multilayer shield

For the analysis of the multilayer shield not has yet been implemented a specifically code. For the 2D a commercial software can be used for investigation of the magnetic field distribution (the magnetic flux density, the magnetic field intensity and the magnetic vector potential) and basic electromagnetic characteristics (inductance and electromagnetic force) [19]. A typical magnetic field problem is described by defining the geometry, material properties, currents, boundary conditions, and the field system equations. The software requires the input dates, the numerical solution of the field equation and output of desired parameters. If the values are found unsatisfactory, the design modified and parameters are recalculated. The process is repeated until optimum values for the design parameters are obtained. The commercial software used in the project is based on the finite element method (FEM) for solving Maxwell's equations and can be used for electromagnetic field modeling, where the field is electrostatics, magnetostatics, eddy currents, time-invariant or time-harmonic and permanent magnets.

The finite elements method assures sufficient accuracy of electromagnetic field computation and very good flexibility when geometry is modeled and field sources are loaded

If the magnetic field is time-varying, eddy currents can be induced in materials with a non-zero conductivity. Several other Maxwell's equations related to the electric field distribution must also be accommodated. Denoting the electric field intensity as E and the current density as J, E and J obey the constitutive relationship:

$$J = \sigma E \qquad (50)$$

The induced electric field then obeys:

$$\nabla \times E = -\frac{\delta B}{\delta t} \qquad (51)$$

Substituting the vector potential form of B into (51) yields:

$$\nabla \times E = -\nabla \times A \qquad (52)$$

In the case of 2-D problems, (52) can be integrated to yield:

$$E = -A - \nabla V \times A \qquad (53)$$

and the constitutive relationship, (50) employed to yield:

$$J = -\sigma A - \sigma \nabla \mathrm{V} \qquad (54)$$

The partial differential equation is obtain:

$$\nabla \times \left(\frac{1}{\mu(B)} \nabla \times \mathrm{A}\right) = -\sigma A + J_{src} - \sigma \nabla \mathrm{V} \qquad (55)$$

where Jsrc represents the applied currents sources. The ∇V term is an additional voltage gradient that, in 2-D problems, is constant over a conducting body. The FEM software uses this voltage gradient in some harmonic problems to enforce constraints on the current carried by conductive regions. The software FEM consider (55) for the case in which the field is oscillating at one fixed frequency. For this case, a phasor transformation yields a steady-state equation that is solved for the amplitude and phase of A. This transformation is:

$$A = Re[a(cos\omega t + jsin\omega t)] = Re\ [ae^{jwt}] \qquad (56)$$

in which A is a complex number. Substituting into (55) and dividing out the complex exponential term yields the equation that the software actually solves for harmonic magnetic problems:

$$\nabla \times \left(\frac{1}{\mu_{eff}(B)} \nabla \times \mathrm{A}\right) = -j\omega\sigma a + J_{src} - \sigma \nabla \mathrm{V} \qquad (57)$$

in which J_{src} represents the phasor transform of the applied current sources. Strictly speaking, the permeability μ should be constant for harmonic problems. However, the software retains a nonlinear relationship in the harmonic formulation, allowing the program to approximate the effects of saturation on the phase and amplitude of the fundamental of the field distribution. The form of the BH curve is derived from "effective permeability" μ_{eff} is selected to give the correct amplitude of the fundamental component of the waveform under sinusoidal excitation. FEMM also allows for the inclusion of complex and frequency-dependent permeability in time harmonic problems. These features allow the program to model materials with thin laminations and approximately model hysteresis effects.

3 Set Up of the laboratory tests

3.1 Generator for the testing of power lines and MV, LV switchgears

3.1.1 Architecture

In order to test in the laboratory sections of electric power lines, MV and LV switchboards is essential to have a generator able to deliver current values relatively high.

With the standard low voltage three phases supply available, we have decided to realize a current transformer with ratio of transformation suitable to generate currents up to 1000A.

A schematic of the device is shown in Figure 19:

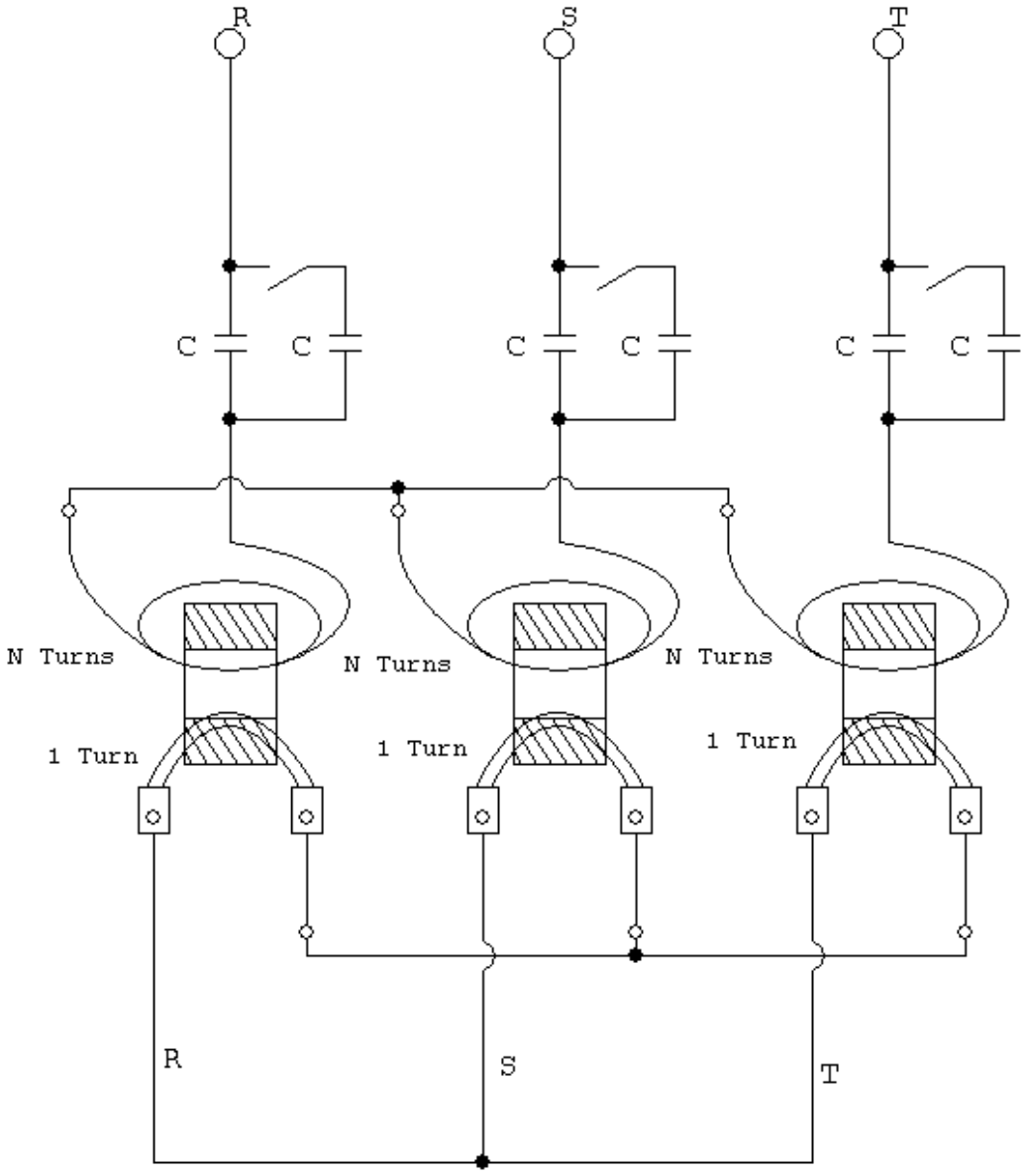

Figure 19 Schematic of the developed transformer

To the secondary of transformer have been connected to equipment under test. The other extremities of the equipment are short-circuited to have a very low impedance and then to be able to generate the required electrical currents. (The electrical load at the secondary of the transformer consists only of the impedance of the line.)
A capacitance is connected at the primary of the transformer to stabilize the electrical load.
Currents in the range 100A to 1000A are required to simulate the entire range of operative conditions of the equipment under test. We have decided for the set of values: 100, 200, 250, 350, 500, 700, 1000 A. The transformer has been developed to have available at the secondary all the currents in the set. With this aim:

- The capacitance for the stabilization of the electrical load is obtained using two capacitors of 30 uF per each phase. One is in series to the windings. The second capacitor is in parallel to the first and it can be connected/disconnected by operating a switch.

- The primary of each phase comprises three windings with different numbers of turns With one 30µF capacitor connected at the primary, the current at the primary is:

$$I = \frac{V}{Z} = \frac{\sqrt{3} \cdot 400}{\frac{1}{2\pi \cdot 50 \cdot 30 \cdot 10^{-6}}} = 2.176 \quad A$$

The number of loops necessary to obtain at the secondary a current equal to 1000 ampere is:

$$N_{Turn} = \frac{I_{wanted}}{I_{\mathrm{Pr}imary}} = \frac{1000}{2.176} \approx 460 \ \ Turns$$

Then, connecting the second capacitor, the number of loops necessary to have 1000A at the secondary is 230. So the use of separate capacitors and windings makes the transformer more flexible. The currents at the primary with one and both capacitors connected are:

- Single capacitor : $I_{1-\mathrm{Pr}imary} = 2.176 \quad A$
- Double capacitor: $I_{2-1\mathrm{Pr}imary} = 4.353 \quad A$

Clearly, with one capacitor and 230 turns, the current at the secondary is 500A.

The three windings of each phase are arranged as in the schematics in Figure 20. The number of turns (N_{Turns}) in each winding has been calculated accordingly to the following procedure:

$$N_{Turns} = \frac{I_{Wanted}}{I_{Primary}}$$

- Winding 1: $N_{1-Turn} = 46$ Turns
- Winding 2: $N_{2-Turn} = 69$ Turns
- Winding 3: $N_{3-Turn} = 115$ Turns

The winding with 46 loops is the first. The other two windings are in series and can be short-circuited to exclude them.

The currents obtained with the different combinations of capacitors and windings are summarized in the following cases and match the desired set of currents at the secondary:

- Winding 1 and only one capacitor connected:

$$I_{sec} = I_{1-Primary} \cdot N_{1-Turn} = 2.176 \cdot 46 = 100\,A$$

- Winding 1 and two capacitors connected:

$$I_{sec} = I_{2-Primary} \cdot N_{1-Turn} = 4.353 \cdot 46 = 200\,A$$

- Winding 1 + Winding 2 and only one capacitor connected:

$$I_{sec} = I_{1-Primary} \cdot (N_{1-Turn} + N_{2-Turn}) = 2.176 \cdot (46 + 69) = 250\,A$$

- Winding 1 + Winding 2 and two capacitor connected:

$$I_{\sec} = I_{2-\mathrm{Pr}imary} \cdot (N_{1-Turn} + N_{2-Turn}) = 4.353 \cdot (46 + 69) = 500\,A$$

- Winding 1 + Winding 3 and only one capacitor connected:

$$I_{\sec} = I_{1-\mathrm{Pr}imary} \cdot (N_{1-Turn} + N_{3-Turn}) = 2.176 \cdot (46 + 115) = 350\,A$$

- Winding 1 + Winding 3 and two capacitor connected:

$$I_{\sec} = I_{2-\mathrm{Pr}imary} \cdot (N_{1-Turn} + N_{3-Turn}) = 4.353 \cdot (46 + 115) = 750\,A$$

- Winding 1 + Winding 2 + Winding 3 and only one capacitor connected:

$$I_{\sec} = I_{1-\mathrm{Pr}imary} \cdot (N_{1-Turn} + N_{2-Turn} + N_{3-Turn}) = 2.176 \cdot (46 + 69 + 115) = 500\,A$$

- Winding 1 + Winding 2 + Winding 3 and two capacitor connected:

$$I_{\sec} = I_{2-\mathrm{Pr}imary} \cdot (N_{1-Turn} + N_{2-Turn} + N_{3-Turn}) = 4.343 \cdot (46 + 69 + 115) = 1000\,A$$

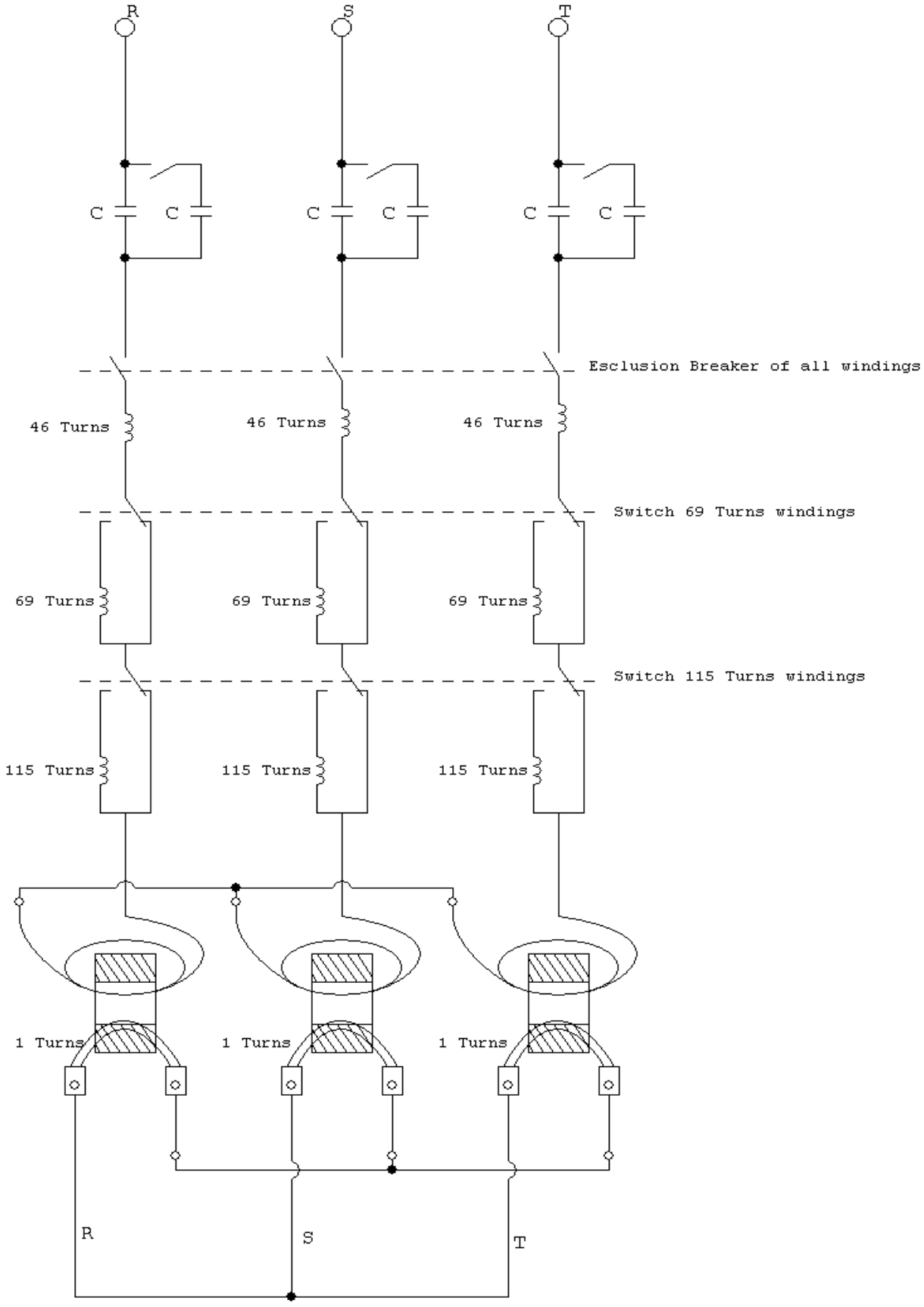

Figure 20 Full electrical scheme of the experimental rig

3.1.2 Realization

After having competed the design phase, the experimental rig has been manufactured and assembled.
The generator consist mainly of two parts:

- The transformer
- The control panel

The overall mass of the testing rig is about 100 Kg. The transformer and the control panel are assembled on a metal plate with four wheels for easy motion and positioning.

3.1.2.1 Transformer

The transformer consists of:

- Three magnetic cores
- Metal Strips
- An insulating layer
- 200 m of 1.5 mm2 electric wire
- Three 300 mm2 stranded wire
- A copper bar
- Five insulator
- An amperometric probe

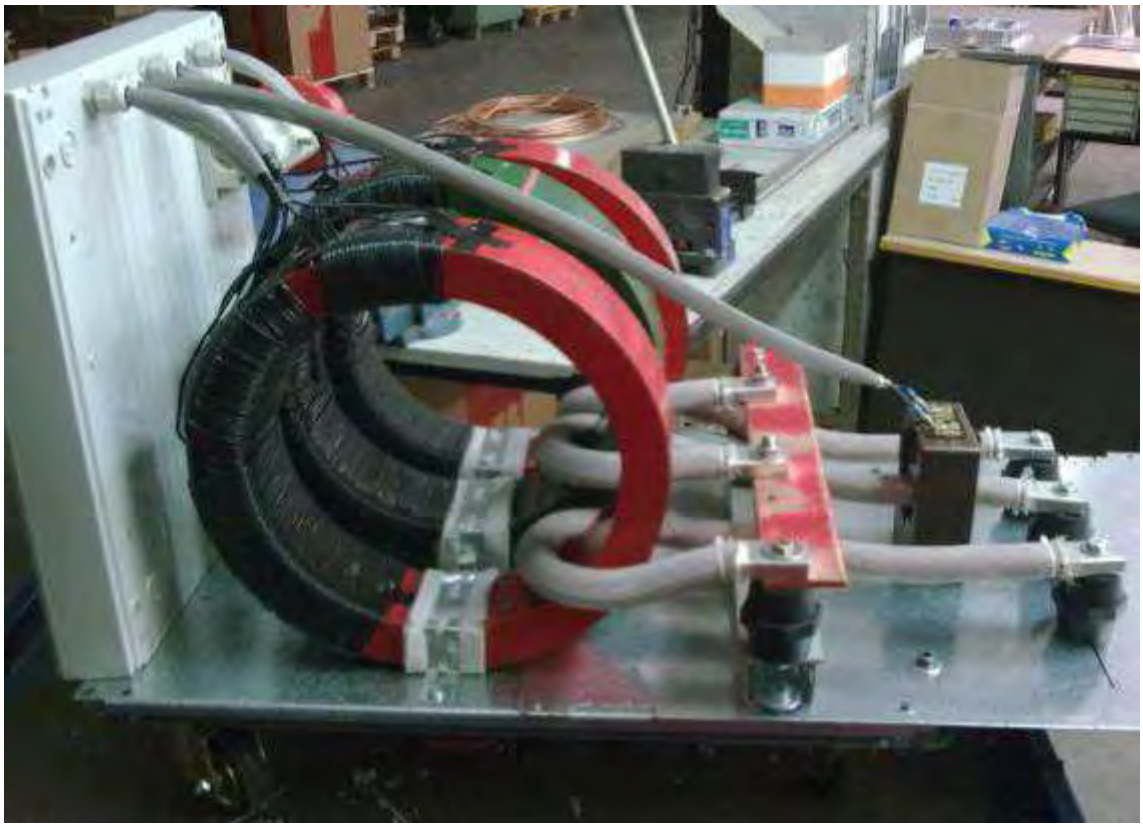

Figure 21 Image of the iron core and of the primary and secondary windings

The magnetic core of each phase is separate from the others and composed of plates electrical insulated with grains oriented (μR =5000). The section of the core is rectangular 30x60 mm. The inner diameter of the core is 300 mm. The external surface is covered with an insulating paint.
First the windings are wound on the cores. Then, the cores are fixed to the frame of the generator using metal strips. Insulating layers are positioned between the extremities of the metal strips and the frame so that they do not form a conductive loop.

After having fixed the cores to the base, the secondary windings are positioned. Each secondary winding is a stranded wire with 300 mm2 section. Both sides of the secondary are insulated from the base plate. One side of each secondary winding is connected to the copper bar to form the connection Wye of the secondary. The other side is connected to the electrical load.

An amperometer is positioned on the control board of the generator and its probe is placed across one of the secondary windings.

3.1.2.2 Control Panel

- Three fuses
- Three 32 A switch
- Two 20 A relay
- Six Capacitor
- An amperometer
- A terminal board
- A pentapolar plug

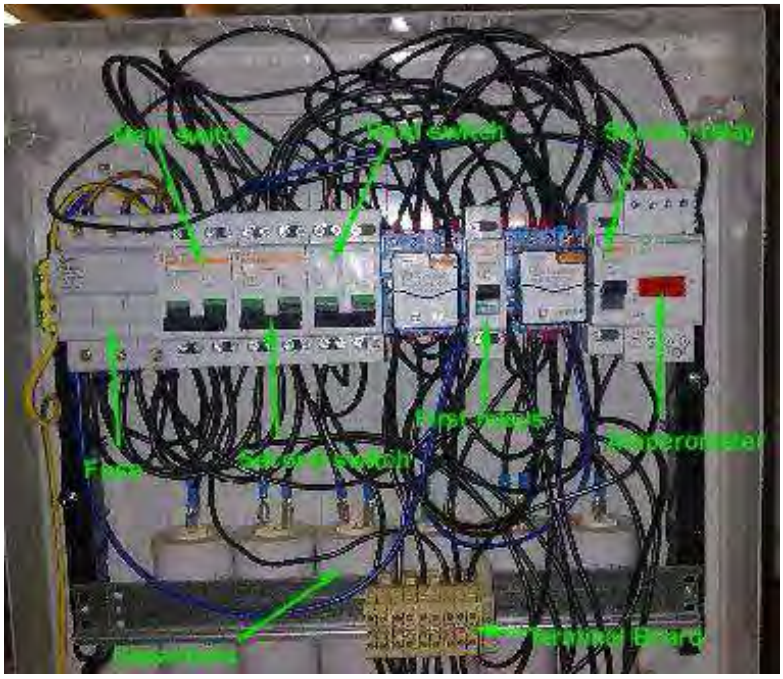

Figure 22 Image of the control board

The 18 extremities of the windings come to a control board where they are connected to the switches and selectors as shown in Figure 22 accordingly to the schematic discussed in the previous section. In the figure, the six capacitors appear on the front bottom.

A for 400 V plug is mounted on the side of the control panel. It is used to power the system.

The control board include a main switch operating on the three phases. Fuses are placed between the plug and the main switch to protect from overvoltage.
From the left, the first switch of the control panel is the main switch. Turning the main switch, for each phase, a capacitors is powered. The second switch is used to connect the other capacitor in

parallel at the first. Six wires connect the six capacitor at the third switch. The third switch power the first winding of each phase and even the other two windings if the relays are switched-off.

The first relays is used like a tripolar selector and is positioned in parallel at the 69 loops winding. When the first relay is switch-on the 69 loops winding is not supplied and the relay is like a short-circuit. Using that configuration is possible to connect the 115 loops winding directly with the 46 loops winding. When the second relay is switch-on the 115 loops winding is not supplied and the relay is like a short-circuit. The not connected terminals, of the 115 loops winding and of the second relay, are connected at the terminal board to form the Wye connection of the primary of transformer.

The power of the electric board was done by inserting a plug on one side of the electric board:

Figure 23 Image of the power point wich powers the control panel

The full control panel looks like in Figure 24

Figure 24 Image of the control panel

3.2 Generator for the testing of MV/LV Transformer

In order to test in laboratory the MV/LV transformer and specifically his magnetic induction, it is very important to use a correct test set up with the objective of the maximization of the secondary current (up to the nominal current of the transformer) and of the minimization of the power delivered at the system under test. To do these a typical test set up of short circuit test was reproduced in laboratory. Two transformers were used, a step up transformer and the transformer under test. The step up transformer have been sized to have a secondary voltage equal to the short circuit voltage of a transformer with primary power at 15 kV and Vdc% of 6% (transformers with these parameters are the most common in the Italian electricity system).

$$V_{1cc} = \frac{V_{1n}}{100} \cdot V_{cc}\% = \frac{15000}{100} \cdot 6 = 900V$$

The step up transformer was then sized to have a secondary voltage of 900 V and a rated power of 100 kVA. This sizing allows to test transformers with power ratings up to 1250 kVA.
This transformer also allows to test transformers with nominal voltages exceeding 15 kV but in this case the nominal current of the transformer under test will be lower the rated.
This component was placed at a distance of 95 meters from the transformer under test in order to not affect the zone of measurement of the magnetic fields.

The electrical diagram show in Figure 25 represents the connections between the two transformers and the protections used. The part of cable that connects the transformers has been twisted to avoid the electromagnetic fields produced by these conductors having influence on the measurement zone.

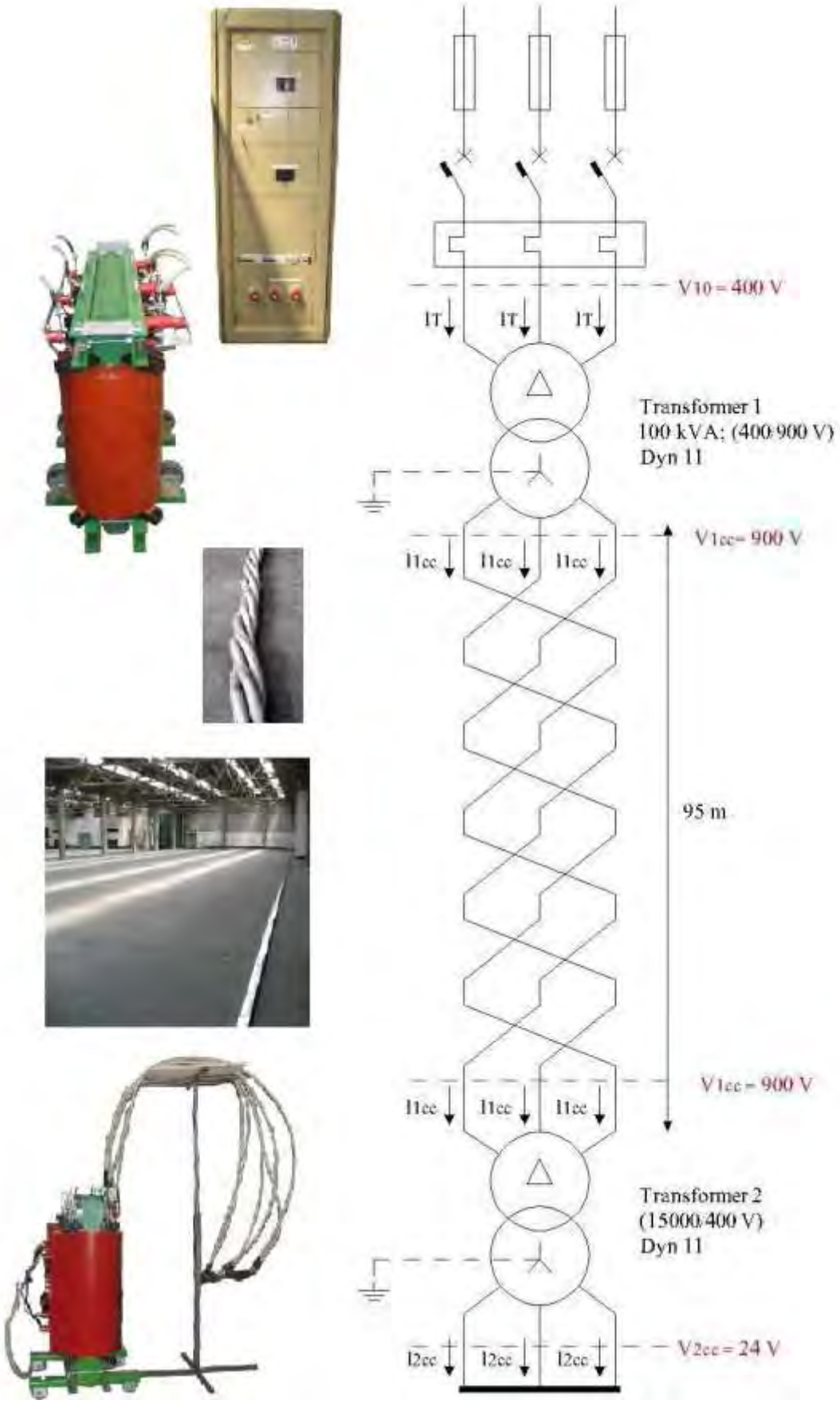

Figure 25 Diagram of the electrical system tested

The step up transformer is not a standard transformer but it is specially built to raise the voltage from 400 V to 900 V with a rated power of 100 kVA:

→ *Constructor: Imefy S.p.a.;*
→ *Model: Cast resin transformer;*
→ *Year built: 2012;*
→ *Rated power: 100 kVA;*
→*Insulation level: 1.1-3 kV/1.1-3kV;*
→ *Rated frequency: 50 Hz;*
→ *Primary winding voltage: 400 V;*
→ *Secondary winding voltage: 900 V;*
→ *Primary winding current: 144.3 A;*
→*Secondary winding current: 64.15A;*
→ *Cooling system: AN;*
→ *Vector group: Dyn11;*
→ *Primary connection: Delta;*
→*Secondary connection: Star +Neutral;*
→*Winding insulation class: F–F;*
→ *IP: 0 0;*
→ *No-load losses at Vn: 451W;*
→*Load losses (115 °C): 581W;*
→*Short circuit voltage(115 °C): 3.5 %;*
→ *No- load current at Vn: 1.2%;*
→ *Weight: 470 Kg;*

Figure 26 Transformer 1; 100 kVA; 400/900 V.

4 Results and Comparisons

In this chapter are reported the results of different configurations that have been analyzed to validate the computation models previously described but also in order to resolve real problems connected at values relatively high of magnetic induction.

In particular, are describe two application examples for each type of shielding analyzed:

• Ferromagnetic shielding

• Conductive shielding

• Mixed shielding

Within the categories listed above were analyzed cases involving the shielding of areas located in close proximity to high voltage power lines, electrical substations MV/LV transformers and electrical switchgear with special features.

The applications analyzed that are described within this elaborate are the following:

- Ferromagnetic shielding:
  - Shielding of a box office of a car wash
  - Shielding of a particular electrical panel
- Conductive shield:
  - Shielding of a public Office under a substation MV/LV
  - Shielding of a typical MV/LV substation of the local distributor [28]
- Mixed shielding
  - Modular shielding system for MV/LV substations [29] [30]
  - Shielding system for a complex substation [31]

The shielding systems described have been implemented in order to verify the accuracy of computational codes and to understand the possible difficulties of application.

4.1 Shielding of a box office of a car wash

In this chapter a ferromagnetic shield system is presented. The objective is the reduction of values of magnetic induction more than 3 μT in a box office that have to be realized over a buried high voltage power line (132 kV). The power line is positioned 3.2 m under the floor of the box office. In Figure 27 is show the layout of the power lines with the geometry of the line. The value of 3 μT is the limit imposed from the Italian legislation for this type of application at a frequency of 50 Hz.

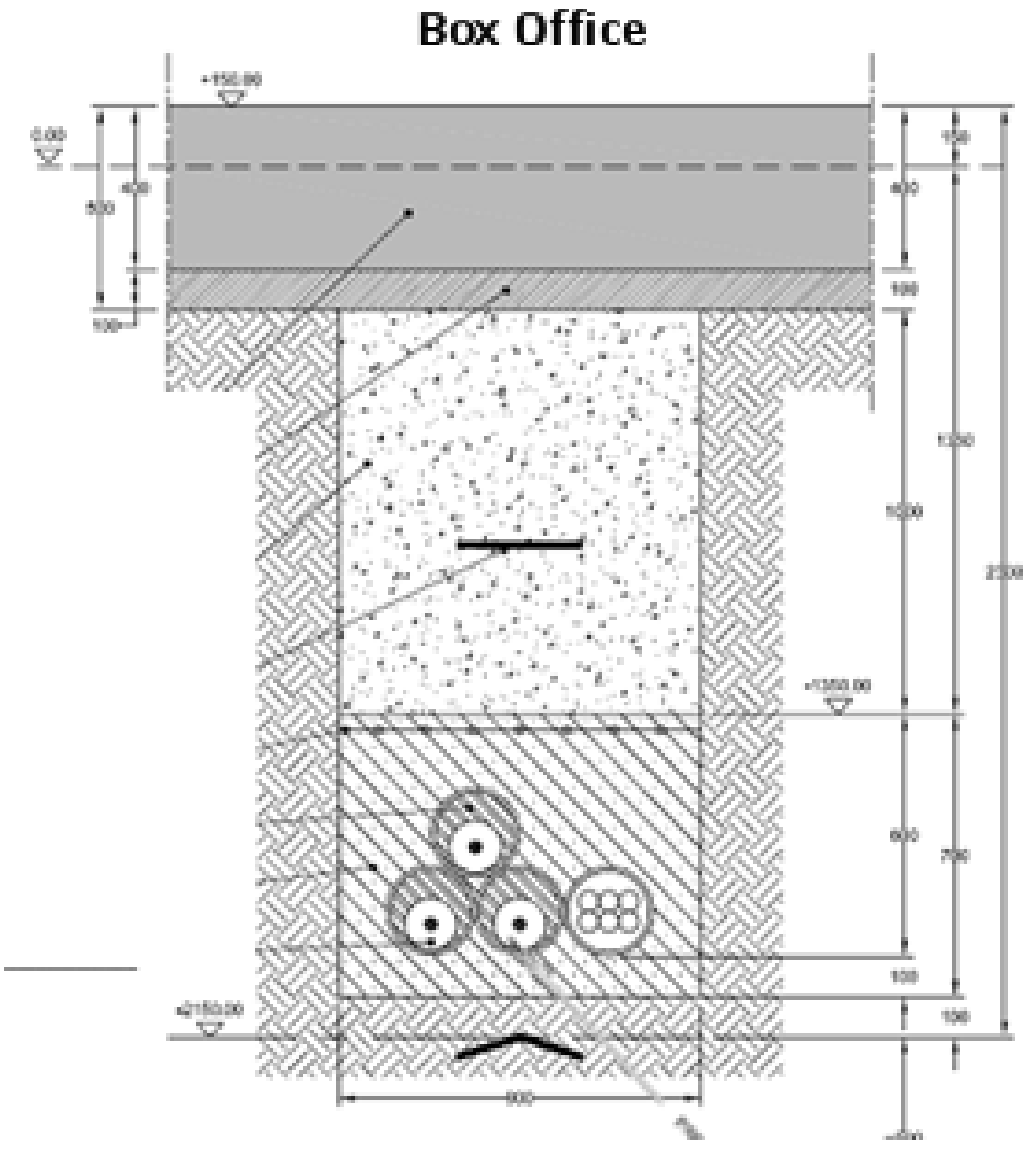

Figure 27 Section of laying the line and of the base

4.1.1 Computation of the values of magnetic induction produced by the line

In order to understand the maximum values of magnetic induction generated by the AT line at 132 kV was carried out a simulation that took into account the geometry of the line and the maximum current flowing in it, set equal to 1000 A.

The results obtained are summarized in Figure 28 where it is possible to see the isolevel lines of magnetic induction in μT calculated on a x-y plane parallel to the walking surface of the area to be protected, with z = 0.5 m.

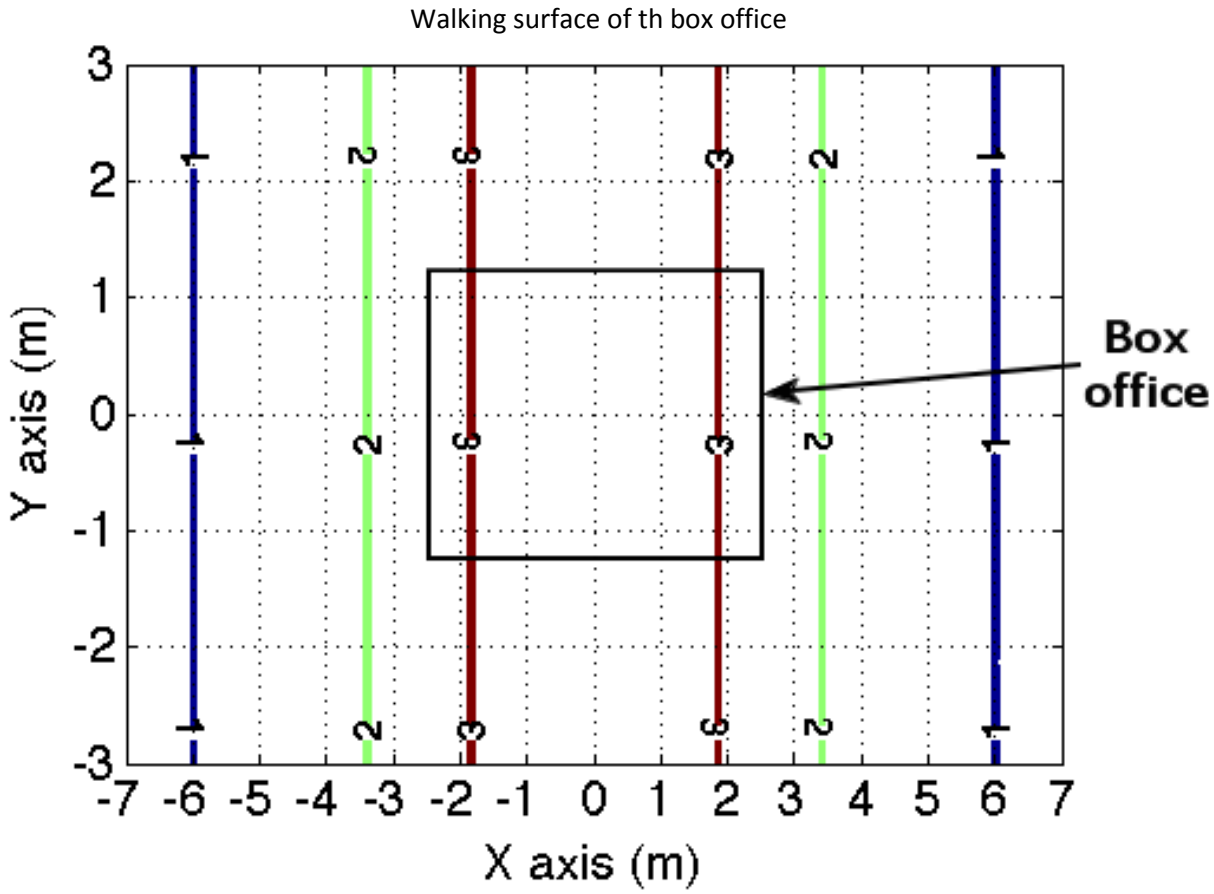

Figure 28 Isolevel lines of magnetic induction calculated at 0.5 m from the walking surface of the box office.

From the graph of Figure 28 it is possible to note how the office area appears almost entirely within the isolevel to 3 μT and consequently in an area in which the limit of 3 μT is exceeded. Consequently it was necessary to design a shielding system able to reduce the values of magnetic induction below the limit of 3 μT even in case of crossing of the maximum current within the line.

4.1.2 Design of the shielding system

For this kind of application the design of the shielding system was carried out using a ferromagnetic material. In particular it was supposed to shield the entire floor of the box office with two laminations of grain oriented silicon steel.

For the simulation have been take into account the property of the material listed below:

- Relative magnetic permeability μ_r= 7500 in the direction of the orientation of the grain
- Relative magnetic permeability μ_r = 1 in the direction perpendicular at the orientation of the grain
- Thickness of each laminations = 0.35 mm
- Number of lamination = 2

The two layers of laminations were simulated with orientation of the grain perpendicular to the axis of the high voltage line.

A shielding system with dimension of 5 x2.5 m have been simulated.

The layout of the shielding system and the relative position from the power line is presented in Figure 29:

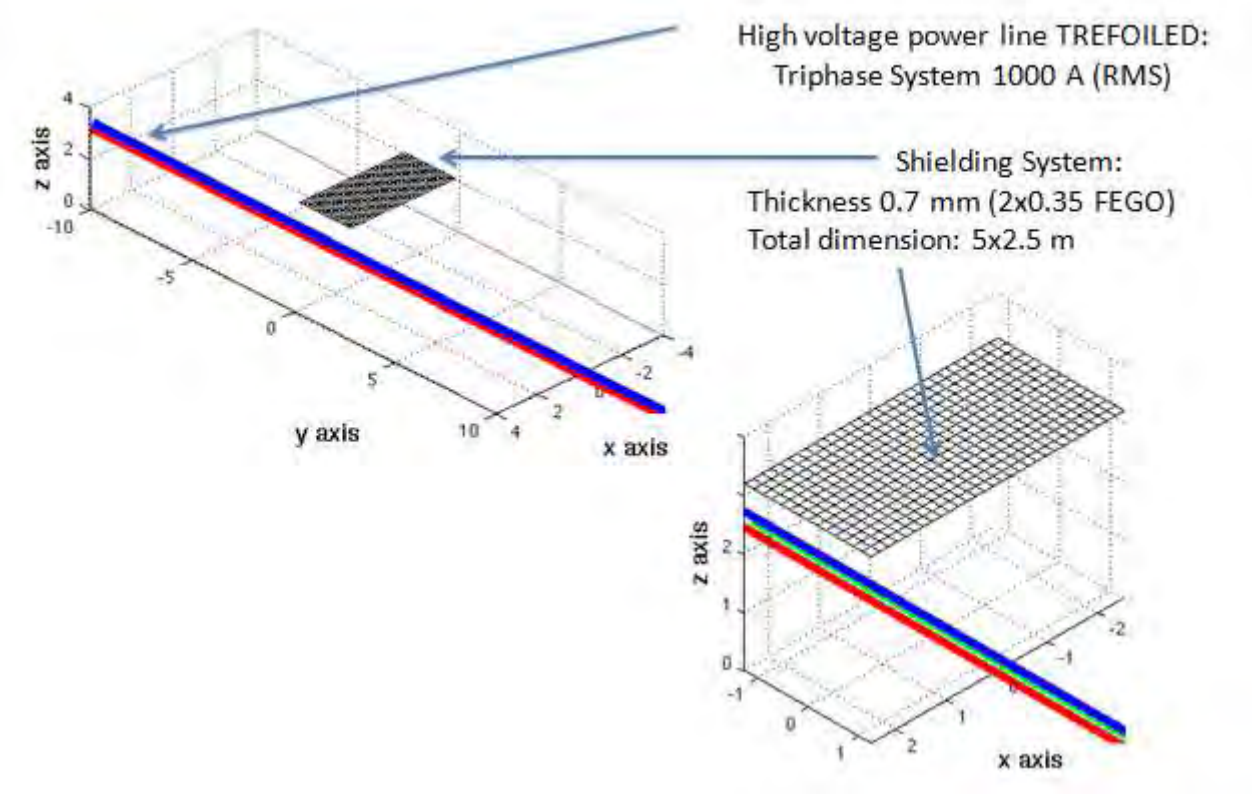

Figure 29 Layout used for the simulations

4.1.3 Result of the simulations

The simulations was carried out using the data listed below. The first result obtain with the simulation is the magnetization of every single domain in which the shielding system have been divided for carrying out the simulation, that is presented in Figure 30:

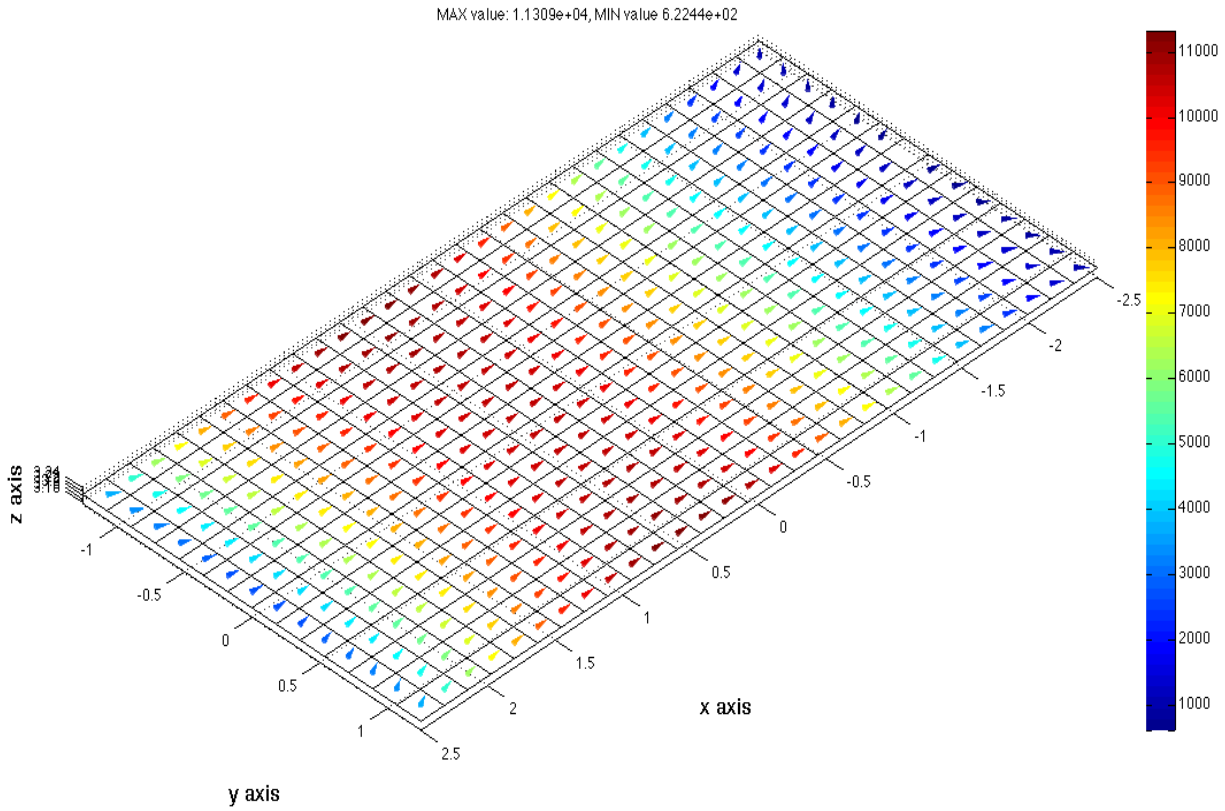

Figure 30 Magnetization of the shielding system

Using the results of the computation of the magnetization is possible to calculate the values of magnetic induction residual as a result of positioning of the screening system.

As expected the shielding system allows to reduce the values of magnetic induction within the box office. In Figure 31 are presented the isolevel lines calculated with the shielding system positioned as show in Figure 29. The isolevel line at 3 μT do not intersect more the area of the box office and so the goal of the shielding system is reached.

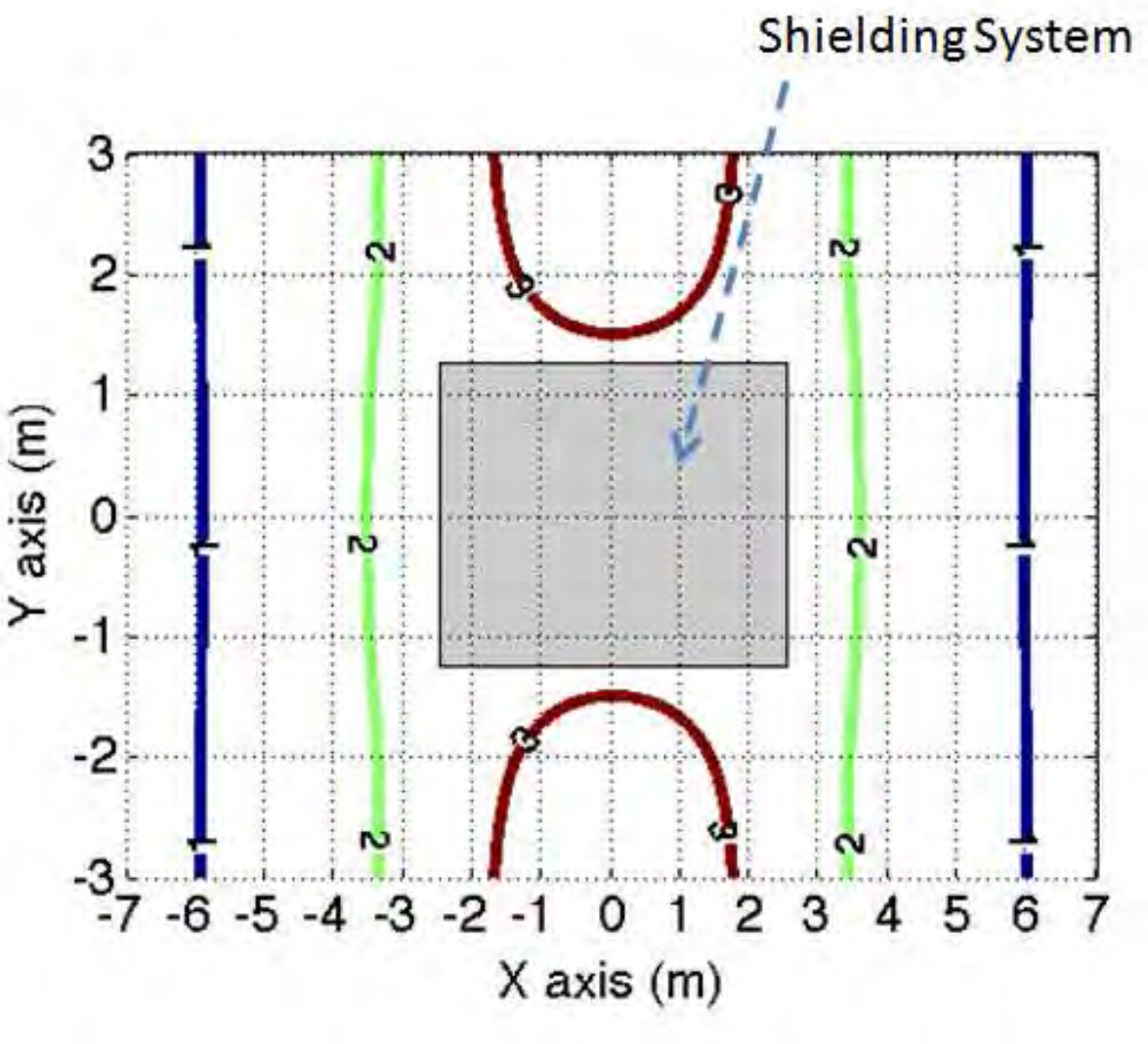

Figure 31 Isolevel lines after the positioning of the shielding system

Comparing the values of magnetic induction calculated in the absence of shielding with those calculated in the presence of shielding has been possible to extract the shielding factor (SF: defined as the ratio between the magnetic induction in the absence and in the presence of the shield) that has been summarized in Figure 32.

The shielding factor obtain with this shielding system is relatively low but enough to reach the objective.

In other application, where a bigger shielding factor is necessary it is possible to enlarge the shielded area or the thickness of the shield.

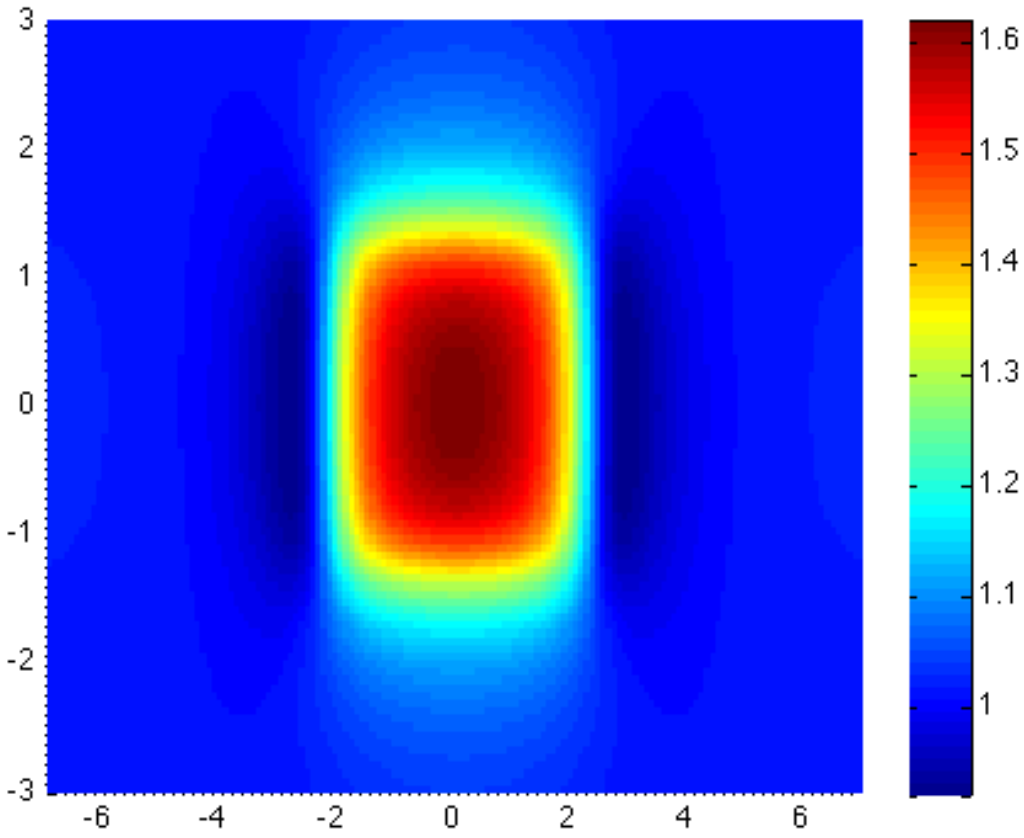

Figure 32 Shielding factor valued for the simulated solution

4.1.4 Implementation of the shielding system

In order to validate the results of the computation the shielding system has been realized and tested. The realization of the shielding has been performed using a small coil of grain oriented silicon steel.

The coil of the width of 1 m, was unrolled and cut in order to cover twice the entire surface to be shielded as presented in Figure 33. The various sheets that make up the shield were overlapped by 10 cm.

Figure 33 Laying the shielding material

The shielding system was fixed on the floor using anchors. The end result of laying is shown in Figure 34

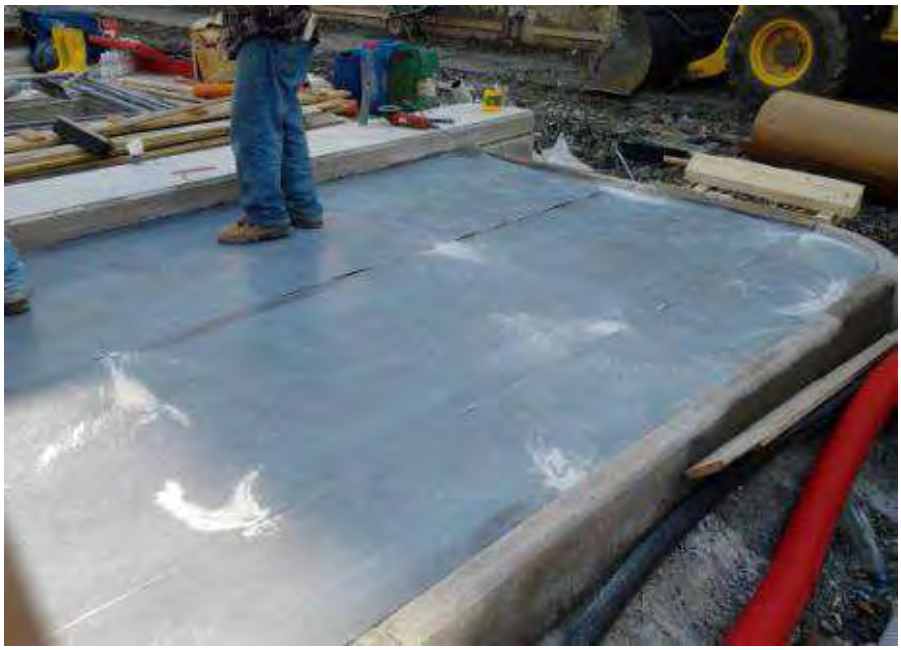

Figure 34 Imagine of the shielding system completed

4.1.5 Check of the shielding factor

The measurement of the levels of magnetic induction was aimed to verify the efficiency of the shielding system installed and was carried out experimentally through a campaign of measurements. Have been compared induction values measured before and after the installation of the shield.

In Italy, the operator of the transmission grid does not provide the data on the instantaneous currents which cross the line and therefore it was decided to perform the detection with two probes. One was positioned above the line (but not in correspondence of the area to shield), sampling the value of magnetic induction every minute. The other probe has been used to sample the values over the area to shield. In this way was monitored the value of magnetic induction in specific points of the area to shield before and after the installation of the shield, and thanks to the probe been fixed, has been possible to understand the variation of the line current at each minute and plot the values measured at various points to the value that would have had if the current had remained constant to the maximum value measured for the duration of sampling.

In Figure 35are shown, in black, the points in which the measurements were performed.

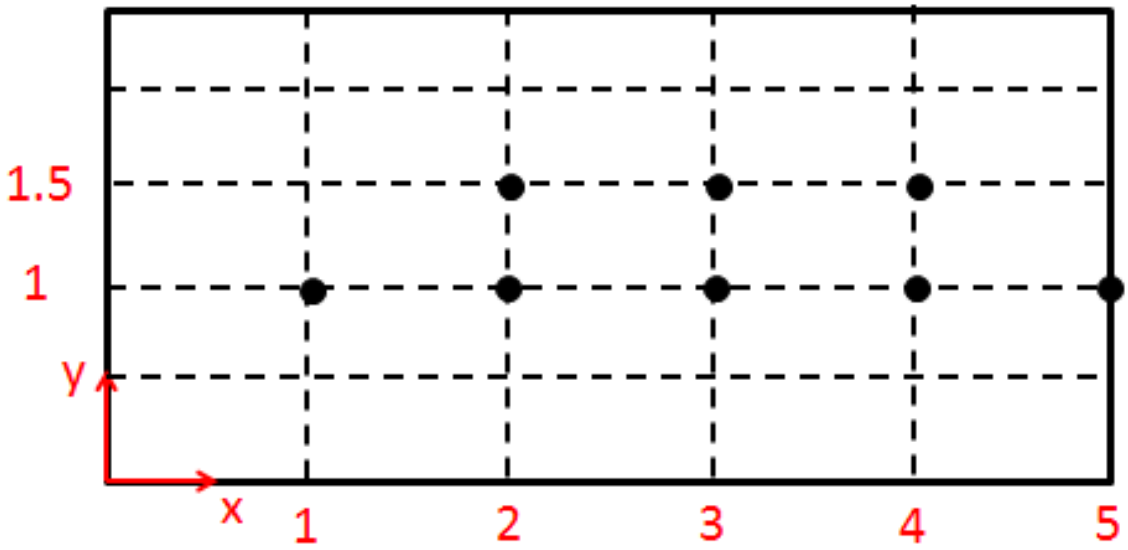

Figure 35 Layout in meter of the measurement points.

4.1.6 Validation of the computation code and conclusion

In order to validate the computation code a comparison was made between the shielding factor obtained from measurements and that one calculated.

The measurement points were grouped into two lines (with z constant equal to 1 m) as shown in the layout of Figure 36.

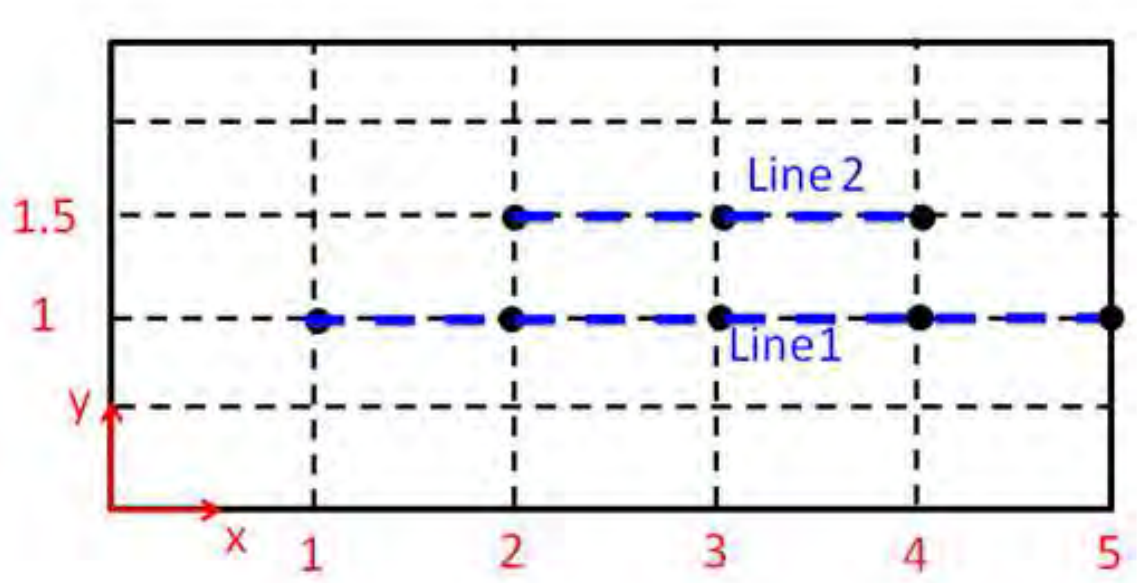

Figure 36 Layout in meter of the lines of comparison

On the two lines presented in Figure 36 the shielding factor have been computed and compared with the one obtained with the measurement. The results of the comparison are summarized in the graph of Figure 37, for line 1, and in the graph of Figure 38 for the line 2.

As can be seen from the two following graphs, the error of the calculation code, with respect to the measured values, is negligible in that it is of the order of 1% on the line 1 and 3% on the line 2.

The calculation model is therefore correct and valid results obtained in the simulations carried out at the design stage. This allows you to ensure the desired objective even at the maximum line current.

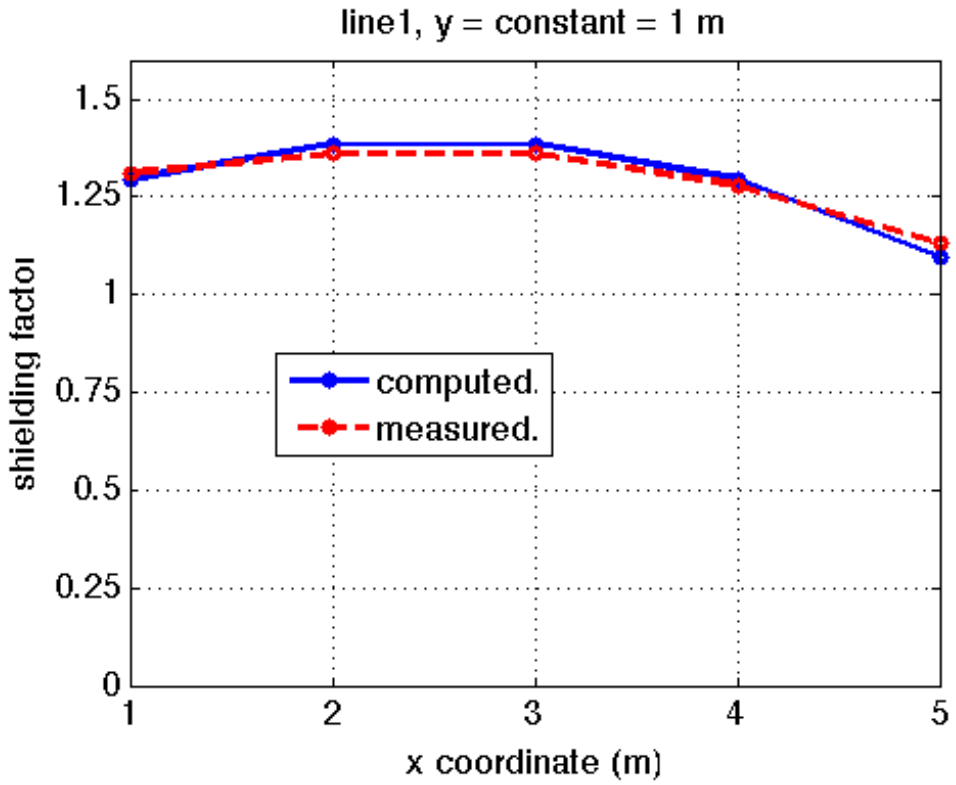

Figure 37 Line 1, comparison between calculated (blue line) and measured (red line) shielding factor

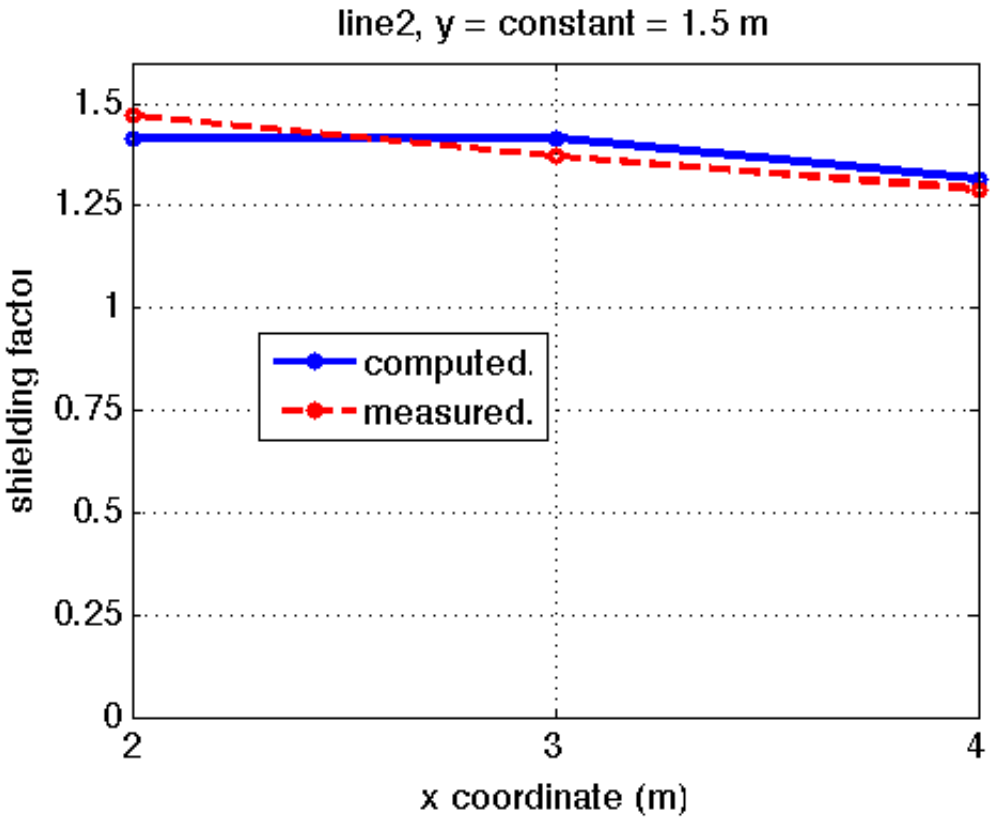

Figure 38 Line 2, comparison between calculated (blue line) and measured (red line) shielding factor

4.2 Shielding of the doors of a particular electrical cabinet

In this chapter a dissertation on a shielding system for a particular electrical cabinet is done. The aim is to present how different property of the materials and different shielding layout influence the final results. The study start from a real case in which a particular electric cabinet have to be shield because generate values of magnetic induction relative high (over 500 μT).

The electric cabinet contain the center point of a big generator of an hydroelectric plant. The center point layout and the relative electric cabinet are presented respectively in Figure 39 and in Figure 40.

Figure 39 Image of the electrical cabinet

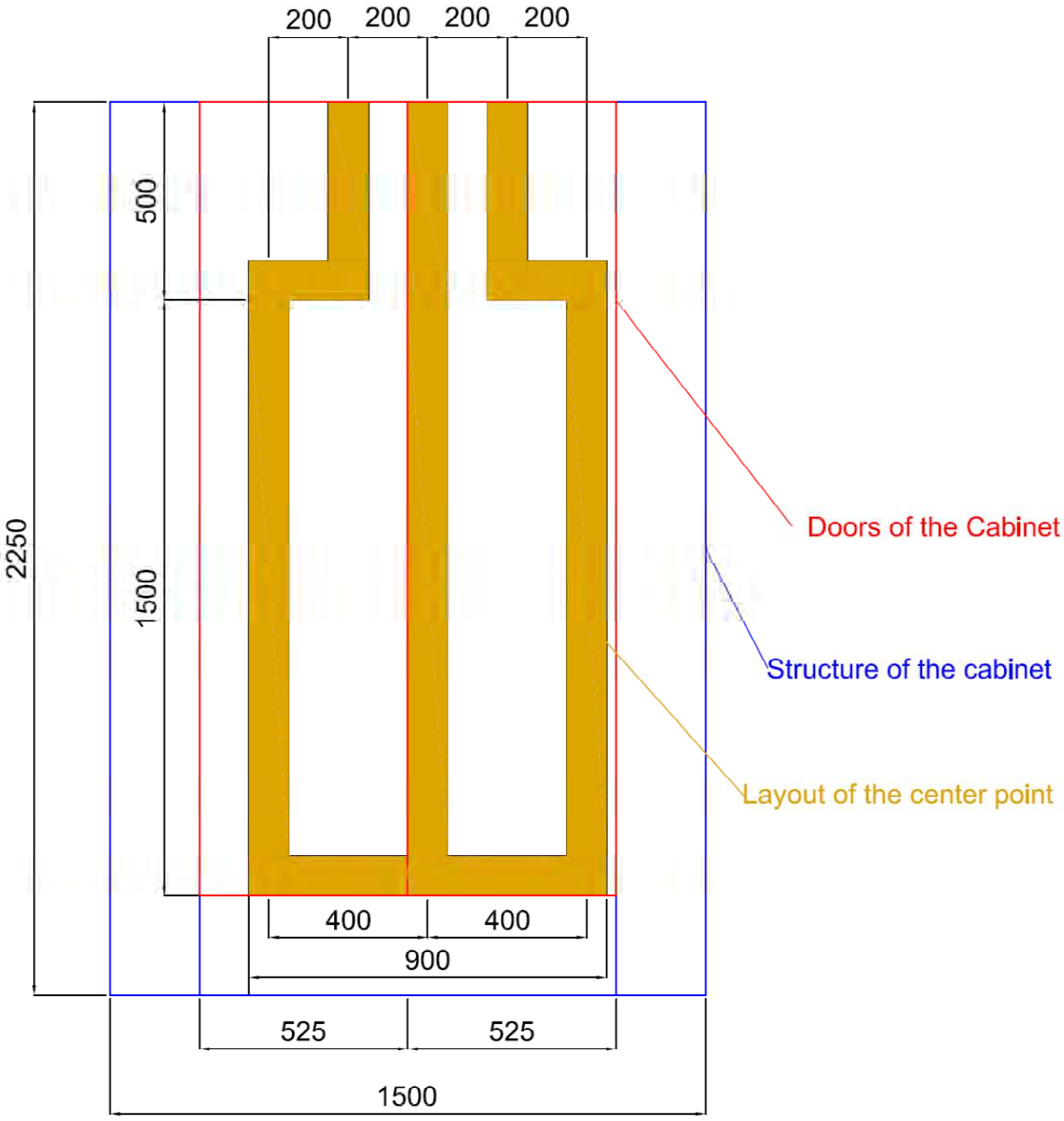

Figure 40 Internal layout of the center point (in yellow), measure in mm

The three vertical yellow segments show in Figure 40 represent the three phase arriving from the generator and the horizontal segment the center point of the phases. The three phases are relatively far one from the other (40 cm) and the nominal current relatively high (2950 A) and this leads to high values of magnetic induction, up to 530 μT at 20 cm from the front of electrical cabinet.

4.2.1 Design of the shielding system

For this kind of application five different configuration of the shielding system have been tested.

- Two plates in front of the electrical cabinet
- Three plates in front of the electrical cabinet
- Shielding u-shaped front closed
- Shielding u-shaped rear closed
- Shielding closed on all 4 sides

In all the configuration listed below an isotropic ferromagnetic material, with relative magnetic permeability μ_r= 7500 and thickness of 0.35 mm have been considered to carry out the simulations.

Another simulation have been performed changing the relative magnetic permeability and the thickness of the plates in order to verify if it would be possible to reduce the weight of the shielding system using a best performing materials. This simulation have been performed considering a material with relative magnetic permeability μ_r= 20000 and thickness of 0.2 mm.

In this case only the shielding layout with two plates in front of the electrical cabinet have been tested.

The five different geometric configuration tested is presented below:

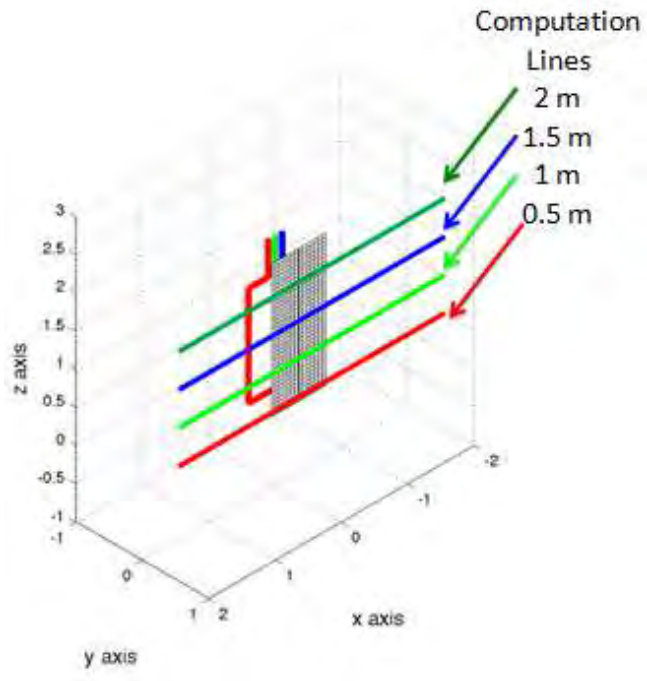

Figure 41 Layout of the shielding system composed of two plates with computation lines and source layout

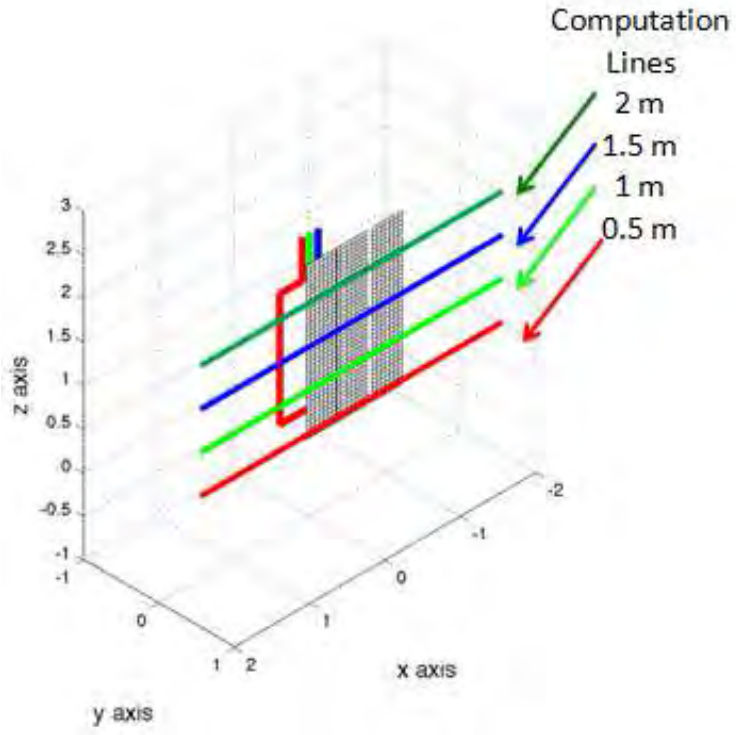

Figure 42 Layout of the shielding system composed of three plates with computation lines and source layout

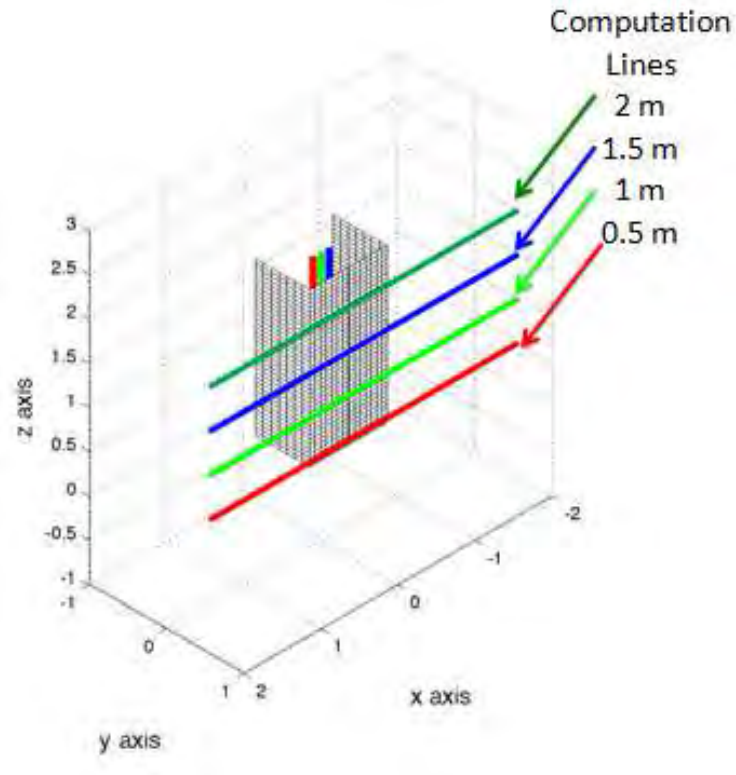

Figure 43 Layout of the shielding system u-shaped front closed with computation lines and source layout

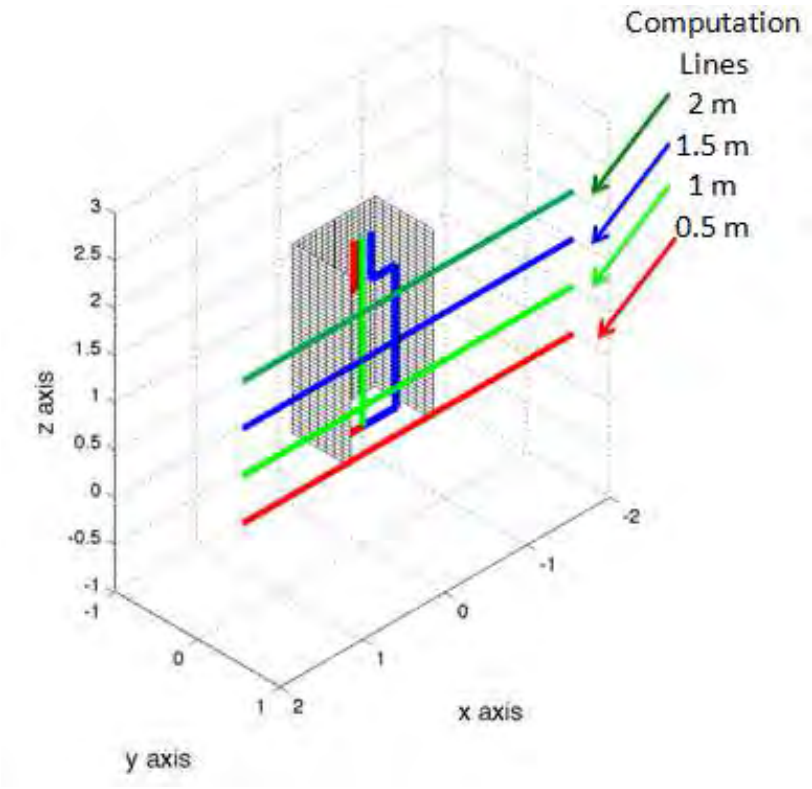

Figure 44 Layout of the shielding system u-shaped rear closed with computation lines and source layout

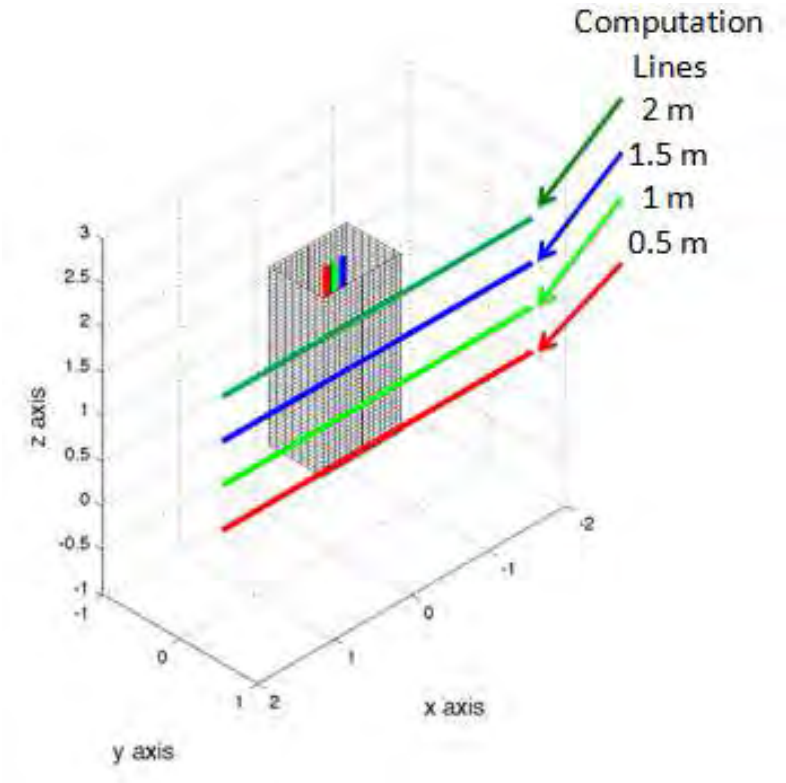

Figure 45 Layout of the shielding system closed on all 4 sides with computation lines and source layout

4.2.2 Result of the simulations

For each case listed before the shielding factor provided by the shield have been calculated on the four computation lines shown in the previous figure. Every computation line is characterized by a specific color in order to present, using the same color, the results obtained on the different four lines in a single figure.

The results obtain for each case are presented below.

- Two plates in front of the electrical cabinet

  This is the start case, the shielded area is relatively small and without lateral appendix. The results obtained are presented in Figure 46

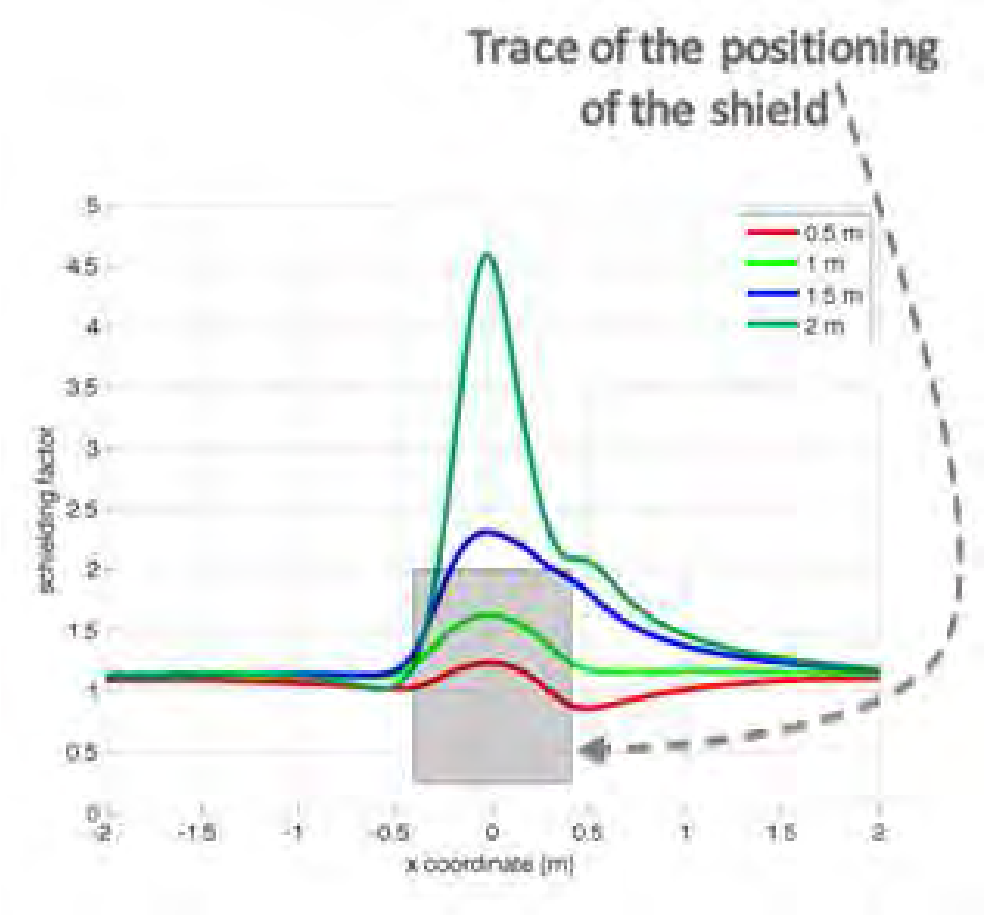

Figure 46 Shielding factor provided by the two plates positioned in front

From the graph of Figure 46 it is clear that the shielding system work better in its upper portion. Probably it is due to the geometry of the source, in fact in the upper part of the electrical cabinet the three conductor of each phase are closely and so the source is smallest than the entire shielding system. Usually a shielding system work better if the shielding system is bigger (in terms of geometrical dimension) respect to the source.

- Three plates in front of the electrical cabinet

  In order to test the hypothesis on the improvement of performance of the screen in case where it is larger than the source was chosen to analyze the case where the screen surface is enlarged by a third. The results obtain with this configuration are presented in Figure 47

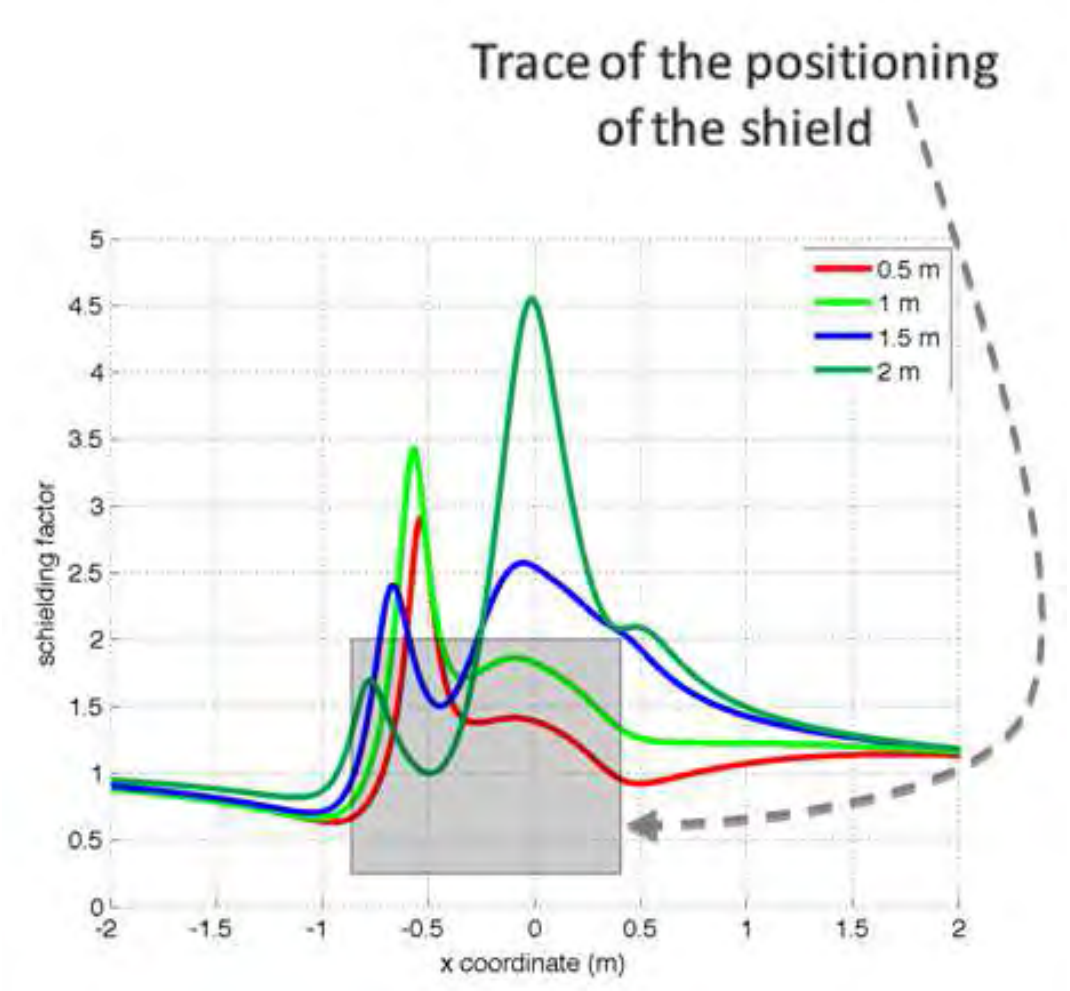

Figure 47 Shielding factor provided by the three plates positioned in front

Analyzing the results presented in Figure 47 is noted an improvement in the shielding factor even on inspection lines closer to the ground while the values for the calculation line is a 2 m remain almost unchanged. This demonstrates how effectively the ratio of the size of the screen and that of the source is a fundamental parameter but this is valid up to a ratio beyond which this improvement is negligible.

Is important to point out that the only direct comparison between the results obtained with the two screen layout can be performed by considering the section with coordinate x: -0.4 to 0.4 m.

Clearly you notice an improvement in the other points covered by the new dimensions of the shield and this improvement is more visible on the lines of inspections closer to the ground.

- Shielding u-shaped front closed

  From the results obtained with the two previous screening systems will note that there is always an important end-effect which cancels the benefits introduced by the screening system at the edges of the shielding system. In order to minimize this problem it was decided to test a screen with two lateral appendixes. The results obtain with this configuration are presented in Figure 48

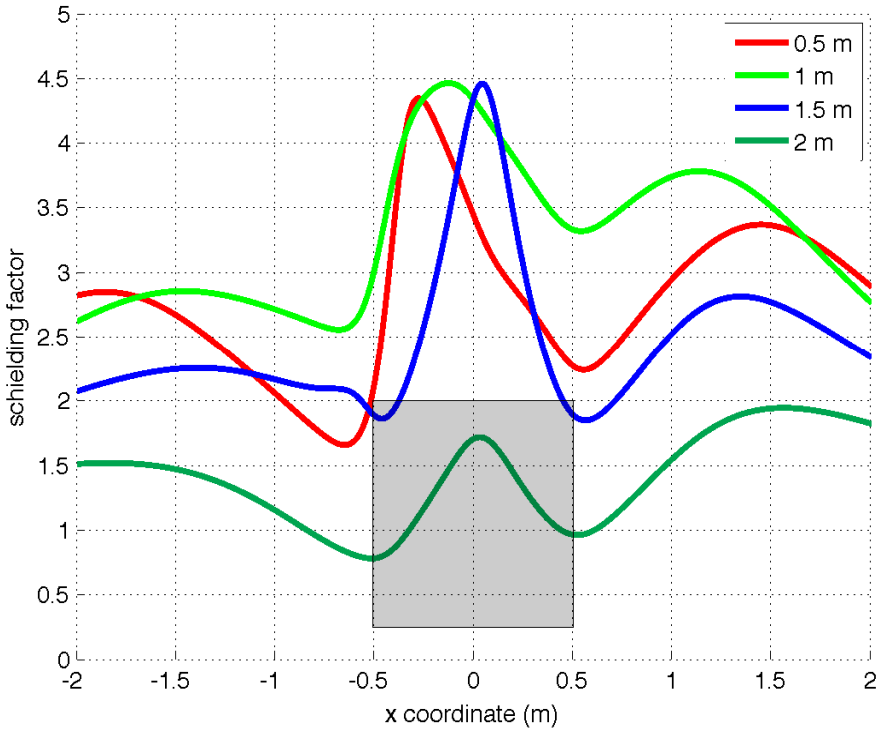

Figure 48 Shielding factor provided by u- shaped shield close in front

From the graph of Figure 48 you notice a significant improvement of the shielding factor with respect to the previous cases. In general the values of SF are grown in all the points of the three inspection lines closest to the ground and especially the SF remains high even in the points which are not in direct correspondence of the screen.

A different assessment must be made for the values calculated to the share of 2 m. In this case the shielding factor drops compared to the previous cases, and this is probably due to a shift of the end effect of the shield.

- Shielding u-shaped rear closed

In order to verify the influence of the ferromagnetic material not directly interposed between the source and the victim, the configuration u-shaped has been tested even with the open part on the victim side.

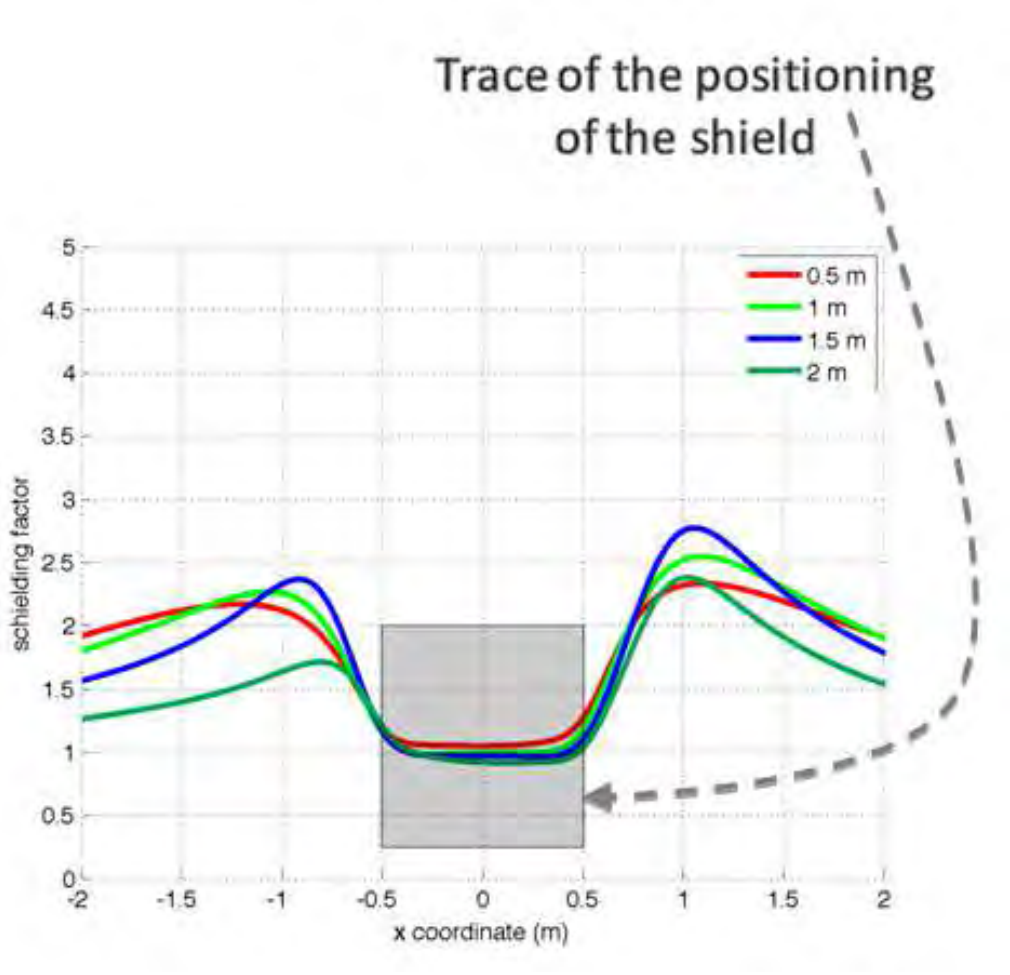

Figure 49 Shielding factor provided by u- shaped shield rear closed